

Enhanced nematic fluctuations near the Mott insulating phase of high- T_c cuprates

Peter P. Orth,¹ Bhilahari Jeevanesan,² Rafael M. Fernandes,³ and Jörg Schmalian^{2,4}

¹Department of Physics and Astronomy, Iowa State University, Ames, Iowa 50011, USA

²Institute for Theory of Condensed Matter, Karlsruhe Institute of Technology (KIT), 76131 Karlsruhe, Germany

³School of Physics and Astronomy, University of Minnesota, Minneapolis, Minnesota 55455, USA

⁴Institute for Solid State Physics, Karlsruhe Institute of Technology (KIT), 76131 Karlsruhe, Germany

The complexity of the phase diagram of the cuprates goes well beyond its unique high- T_c superconducting state, as it hosts a variety of different electronic phenomena, such as the pseudogap, nematic order, charge order, and strange metallic behavior. The parent compound, however, is well understood as a Mott insulator, displaying quenched charge degrees of freedom and low-energy antiferromagnetic excitations described by the Heisenberg exchange coupling J . Here we show that doping holes in the oxygen orbitals inevitably generates another spin interaction – a biquadratic coupling – that must be included in the celebrated $t - J$ model. While this additional interaction does not modify the linear spin wave spectrum, it promotes an enhanced nematic susceptibility that is peaked at a temperature scale determined by J . Our results explain several puzzling features of underdoped $\text{YBa}_2\text{Cu}_3\text{O}_7$, such as the proximity of nematic and antiferromagnetic order, the anisotropic magnetic incommensurability, and the in-plane resistivity anisotropy. Furthermore, it naturally accounts for the absence of nematicity in electron-doped cuprates, and supports the idea that the pseudogap temperature is related to strong local antiferromagnetism.

Introduction. Hole-doped cuprates are susceptible to a variety of different types of electronic order in the underdoped regime [1, 2]. Examples include charge order [3–6], which becomes long-ranged in the presence of large magnetic fields [3, 6], and nematic order [7–11], which seems to be stabilized only in compounds whose lattice structures explicitly break the tetragonal symmetry of the system [12, 13]. While such a complexity might, at first glance, suggest that there is no universal explanation for the rich physics of hole-doped cuprates, two important guiding principles emerge from the analysis of their phase diagram (see Fig. 1): (i) novel phases other than superconductivity only appear below the ubiquitous pseudogap temperature T^* ; (ii) $T^*(x)$ monotonically increases as one moves closer to the parent compound ($x = 0$), approaching values of several hundreds of Kelvin, comparable therefore to the antiferromagnetic (AFM) transition temperature of the parent compound.

This observation suggests a close connection between the pseudogap and AFM correlations [14–16]. Near $x = 0$, these AFM correlations arise from the well-understood Mott (or more precisely, charge-transfer [17]) insulating state of the parent compound. Such a connection between pseudogap and AFM [18] is consistent with the recent observation of a sudden change of the effective carrier number from x to $1 + x$ near the doping level where T^* drops rapidly [19], or at a fixed doping level when T^* is crossed [20]. Furthermore, it provides an interesting guiding principle to understand the tendencies towards the different types of electronic order below T^* as also arising from strong AFM correlations.

In this context, several recent works have proposed that charge order arises from magnetic fluctuations [21–23]. In this paper, we demonstrate that nematic order – an electronic order that breaks the tetragonal symme-

try of the CuO_2 plane [24] – is closely related to strong short-range AFM fluctuations as well. The key new ingredient of our approach to underdoped cuprates is the

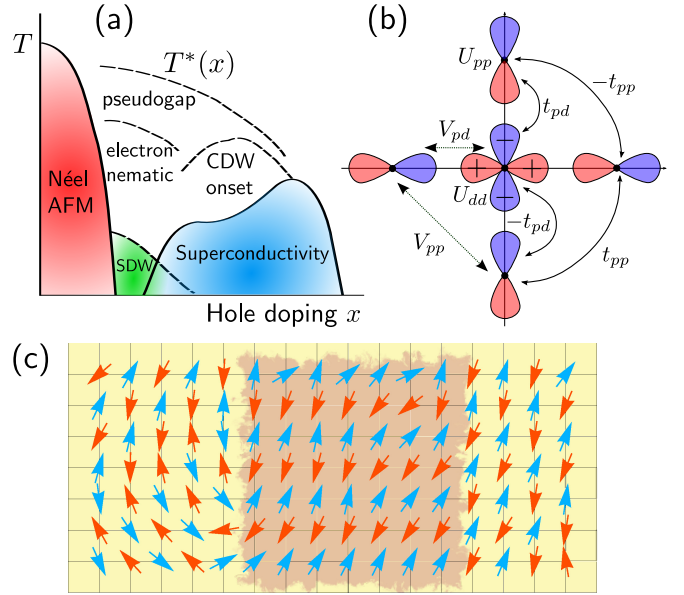


FIG. 1. Microscopic manifestation of nematic fluctuations. (a) Schematic phase diagram of hole-doped cuprate superconductors. (b) The microscopic model contains a Cu $3d_{x^2-y^2}$ orbital (center orbital) and O $2p_x$ and $2p_y$ orbitals in a single unit cell. The hopping parameters are given by t_{pd}, t_{pp} and the interactions consist of on-site U_{dd}, U_{pp} and nearest-neighbor V_{pd}, V_{pp} . (c) Nematic fluctuations induce a short-ranged magnetic stripe ordered region (light red) within a Néel ordered background (yellow), as seen in our Monte Carlo simulations. Red and blue color of the arrows denote out-of-the-plane components of the spins.

generalized $t - J - K$ model:

$$H_{t-J-K} = \sum_{ij\alpha} t_{ij} \tilde{d}_{i\alpha}^\dagger \tilde{d}_{j\alpha} + J \sum_{\langle ij \rangle} \left(\mathbf{S}_i \cdot \mathbf{S}_j - \frac{1}{4} n_i n_j \right) - K \sum_i [\mathbf{S}_i \cdot (\mathbf{S}_{i-\hat{x}} + \mathbf{S}_{i+\hat{x}} - \mathbf{S}_{i-\hat{y}} - \mathbf{S}_{i+\hat{y}})]^2. \quad (1)$$

The first two terms comprise the standard $t - J$ model widely employed to describe lightly hole-doped Mott insulators [25], with t_{ij} denoting the hole hopping parameters and J the AFM exchange coupling (weaker, longer range Heisenberg interactions are possibly included as well). The operator $\mathbf{S}_i = \frac{1}{2} \sum_{\alpha\beta} \tilde{d}_{i\alpha}^\dagger \boldsymbol{\sigma}_{\alpha\beta} \tilde{d}_{i\beta}$ describes the Cu spin and $n_i = \sum_{\alpha} \tilde{d}_{i\alpha}^\dagger \tilde{d}_{i\alpha}$ the corresponding charge. The strong local Coulomb interaction is incorporated in terms of the Cu-hole creation operator $\tilde{d}_{i\alpha}^\dagger = (1 - n_{i\bar{\alpha}}) d_{i\alpha}^\dagger$, reflecting the fact that double occupancy of the sites is not allowed. The new term here is the biquadratic exchange term H_K (the last term in Eq. (1)) which is governed by the coupling constant $K > 0$. As we derive below and show in Fig. 2(a), H_K is naturally induced by non-critical charge fluctuations on the oxygen orbitals, which in turn affect the interaction between neighboring Cu-spins; K is also enhanced by the oxygen-oxygen Coulomb repulsion. We note that the importance of O degrees of freedom for the nematic state of the cuprates has been pointed out in several interesting previous works [26–30].

Using Monte Carlo and analytical methods, we find as shown in Fig. 2(b,c) and Fig. 3, that the main consequence of H_K is to enhance the static electronic nematic susceptibility χ_{nem} near the AFM-Mott insulating state. However, χ_{nem} is not found to diverge on its own. Consequently, within the $t - J - K$ model, the onset of nematic order requires an additional symmetry breaking field that can take advantage of the enhanced susceptibility. It is natural that the CuO chains in YBa₂Cu₃O₇ (YBCO) play exactly this role of a symmetry breaking field. Such a scenario is supported by the experiments, which seem to constrain nematic order to compounds in which the tetragonal symmetry is explicitly broken [13]. The enhanced nematic susceptibility is however present in underdoped cuprates with fully intact tetragonal symmetry and can be determined via elastoresistance measurements [31]. Below we make a prediction for the outcome of such a measurement. We note that an enhanced nematic response was previously reported for the single-orbital Hubbard model in both weak-coupling [32] and strong-coupling [33] regimes. Our analysis implies that the inclusion of oxygen states strongly amplifies this behavior.

The nematic order resulting from H_K explains the momentum anisotropy and the incommensurability of the spin-spin correlation function observed by neutron scattering in the paramagnetic phase of YBCO [8, 34], as

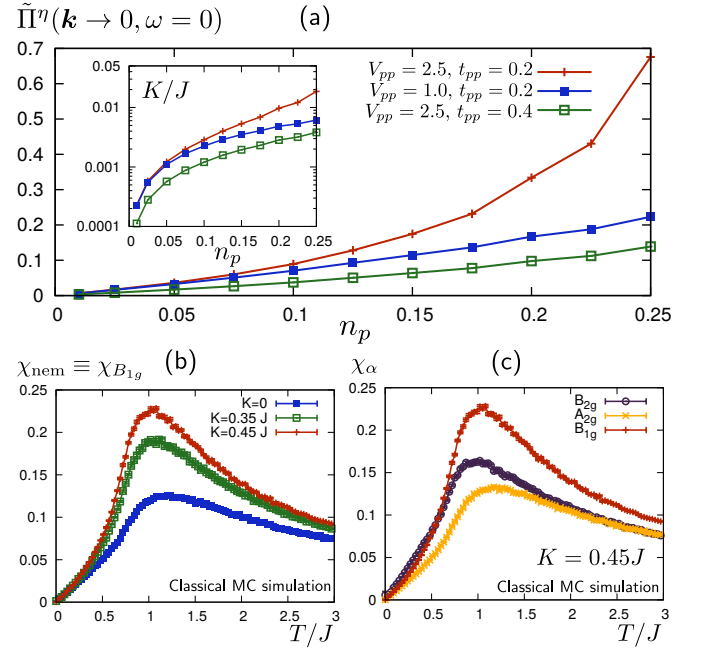


FIG. 2. Strength of biquadratic exchange K within three-band model and enhanced nematic spin fluctuations obtained via Monte Carlo simulations. Panel (a) shows the renormalized quadrupolar response $\tilde{\Pi}^\eta \equiv \frac{1}{2} [(\Pi_{\mathbf{k}=0}^\eta)^{-1} - U_{\mathbf{k}}]^{-1}$ as a function of the oxygen density n_p obtained within the three-band model at low temperature $T = 10^{-2} t_{pp}$ and fixed $n_d = 1$. Other parameters are $t_{pd} = 1$, $\Delta = 2.5$, $U_{dd} = 9$, $U_{pp} = 3$, $V_{pd} = V_{pp}$. Oxygen quadrupolar fluctuations increase with V_{pp} and smaller oxygen bandwidth t_{pp} . The inset shows the resulting value of $K/J \propto (J'^2/J)(n_p/t_{pp})$ from which we conclude that enhancement of fluctuations by V_{pp} is crucial for a significant biquadratic exchange. We take a Hartree mean-field shift of $\Delta_{\text{eff}} = \Delta + 2n_p(V_{pp} - V_{pd} - U_{pp}/8)$ into account when calculating J' , J . Panels (b-c) show the static nematic susceptibility χ_{nem} in Eq. (5) for the H_{t-J-K} model of Eq. (1) at half-filling as a function of temperature T obtained by Monte Carlo (MC) simulations of classical spins. A non-zero K enhances the response in the nematic B_{1g} channel only. For consistency with the known spin-wave spectrum, we consider a small ferromagnetic next-nearest-neighbor exchange $J_2 = -0.1J$.

well as the direction of the magnetic moment inside the AFM ordered state [35]. Scattering by these anisotropic fluctuations also address another hallmark of the nematic phase, namely, the in-plane resistivity anisotropy [7, 36]. Furthermore, because H_K is the result of charge fluctuations on the oxygen orbitals, it is only present in the hole-doped side of the phase diagram, since electron-doping adds charge carriers directly to the Cu sites [37]. This property is again consistent with experiments, which, to the best of our knowledge, have not reported nematic correlations in electron-doped cuprates [12].

Microscopic model. Our starting point is the three-orbital Hubbard model of the CuO₂-planes $H = H_0 + H_U + H_V$ [38, 41], which includes the $3d_{x^2-y^2}$ Cu or-

bital with creation operator $d_{i\sigma}^\dagger$ at position \mathbf{R}_i and spin σ as well as the $2p_x$ and $2p_y$ O orbitals (see Fig. 1(b)) with creation operators $p_{i+\frac{x}{2}\sigma}^\dagger$ and $p_{i+\frac{y}{2}\sigma}^\dagger$. The non-interacting part H_0 includes hopping between oxygen orbitals (with amplitude t_{pp}) and between copper and oxygen orbitals (with amplitude t_{pd}). The corresponding sign factors of the hopping elements follow from the phases of the orbitals as shown in Fig. 1(b), see Ref. [38]. In addition H_0 contains on-site terms where the energy difference between Cu and O orbitals is given as $\Delta = \varepsilon_p - \varepsilon_d$. We further include on-site interactions $H_U = \sum_i (U_{dd} n_{i\uparrow}^d n_{i\downarrow}^d + \frac{U_{pp}}{2} n_{i\uparrow}^p n_{i\downarrow}^p)$ with $n_{i\sigma}^d = d_{i\sigma}^\dagger d_{i\sigma}$ and $n_{i\sigma}^p = p_{i\sigma}^\dagger p_{i\sigma}$ as well as nearest-neighbor interactions $H_V = \frac{V_{pp}}{2} \sum_{i,u} n_i^p n_{i+u}^p + V_{pd} \sum_{i,u} n_i^d n_{i+u}^p$ with $n_i^{p/d} = \sum_\sigma n_{i\sigma}^{p/d}$.

The energy scales are the local repulsion U_{dd} at the Cu-sites and the charge-transfer energy Δ (with U_{dd} much larger than Δ), suggesting a strong coupling expansion in small $t_{ij} \ll \Delta, U_{dd} - \Delta$. This yields a description in terms of localized Cu spins \mathbf{S}_i coupled to mobile O holes. An expansion up to fourth order in the hopping term t_{pd} was performed in Ref. [39]. There appear (for details see the Supplementary Material (SM) [41]) Kondo-like exchange couplings $\propto \mathbf{S}_i \cdot \mathbf{s}_{jk}$ between Cu and O spin-densities, $\mathbf{s}_{jk} = \frac{1}{2} \sum_{\alpha\beta} p_{j\alpha}^\dagger \sigma_{\alpha\beta} p_{k\beta}$, a Heisenberg exchange term $J \sum_{\langle i,j \rangle} \mathbf{S}_i \cdot \mathbf{S}_j$, and, most notably for our considerations, a spin exchange term that depends on the occupation of the intermediate oxygen orbital between copper sites:

$$H_{J'} = -J' \sum_{i,\delta} n_{i+\frac{\delta}{2}}^p \mathbf{S}_i \cdot \mathbf{S}_{i+\delta} \quad (2)$$

where $\delta = \{\pm\hat{x}, \pm\hat{y}\}$ and the coupling constant is given by $J' = \sum_{n=0}^3 \frac{t_{pd}^4 \text{sign}(3-2n)}{\Delta^{3-n} (U_{dd} - \Delta)^n}$. Note that $J = \sum_{n=0}^2 \frac{t_{pd}^4 (4-n^2-\delta_{n,2})}{2\Delta^{3-n} (U_{dd} - \Delta)^n}$ and in the large- U_{dd} limit $J'/J \rightarrow 1/2$. Oxygen charge fluctuations thus not only renormalize the Heisenberg exchange via the Kondo coupling terms, but, as we show now, also lead to the biquadratic spin exchange interaction K in Eq. (1). This follows from decomposing the oxygen densities as $n_{i+\frac{\delta}{2}}^p = n_i^p + \eta_i$ and $n_{i+\frac{\delta}{2}}^p = n_i^p - \eta_i$, where η_i is the quadrupolar (nematic) component of the oxygen charge density [27]. The combination of O on-site and nearest-neighbor Coulomb interactions leads to a term $(-2 \sum \mathbf{U}_k \eta_{\mathbf{k}} \eta_{-\mathbf{k}})$ in the Hamiltonian, where $\mathbf{U}_k = \frac{1}{4} (V_{pp} \text{Re} f_{\mathbf{k}} - \frac{U_{pp}}{2})$ and $f_{\mathbf{k}} = 1 + e^{-ik_x} + e^{ik_y} + e^{i(k_y - k_x)}$. Note that the observed charge density order of the cuprates has been interpreted as being dominated by a quadrupolar form factor of this type [3, 4], suggesting that it may be related to a condensation of the Fourier transform $\eta_{\mathbf{q}}$ of η_i at a finite momentum [43]. In what follows we do not focus on this closely related ordered state, but integrate out the quadrupolar oxygen charge fluctuations. The details of this analysis are

summarized in the SM [41] and yield the result for the biquadratic exchange interaction in Eq. (1)

$$K = \frac{J'^2}{2} \lim_{\mathbf{k} \rightarrow 0} \frac{\Pi_{\mathbf{k}}^\eta}{1 - U_{\mathbf{k}} \Pi_{\mathbf{k}}^\eta} > 0. \quad (3)$$

Here, $\Pi_{\mathbf{k}}^\eta = -\int_{\mathbf{q}, \omega'} \text{Tr}[G_{\mathbf{q}, \omega'}^p(\tau^z \sigma^0) G_{\mathbf{q}+\mathbf{k}, \omega'}(\tau^z \sigma^0)]$ is the bare oxygen charge susceptibility in the quadrupolar (i.e. nematic) channel. The Pauli matrices σ_i and τ_j act in spin and p_x, y -orbital space, respectively. Explicit expressions for the oxygen Green's functions $G_{\mathbf{q}, \omega}^p$ are given in [41] and yield $\Pi_{\mathbf{k}=0}^\eta = 2 \int_{\mathbf{q}} \frac{n_F(\xi_-) - n_F(\xi_+)}{\epsilon_{\mathbf{q}}}$ with $\xi_{\pm} = \pm \epsilon_{\mathbf{q}} - \mu$ and $\int_{\mathbf{q}} \equiv \int_{\text{BZ}} \frac{d^2 q}{(2\pi)^2}$. Here, $\epsilon_{\mathbf{q}}$ is the (effective) oxygen dispersion and μ the chemical potential. Eq. (3) makes it clear that the biquadratic exchange in Eq. (1) is a natural consequence of quadrupolar oxygen charge fluctuations.

The oxygen quadrupolar susceptibility $\Pi_{\mathbf{k}=0}^\eta$ (and thus K) is positive and determined by the occupation number difference between the upper and lower oxygen bands. In the relevant regime of small hole fillings $n_p \ll 1$, the response approaches a constant $\Pi_{\mathbf{k}=0}^\eta \propto n_p$ at low T , peaks around $T \approx |\mu|$ and vanishes as $1/T$ at large T . In Fig. 2(a) we present results for the renormalized quadrupolar response $\tilde{\Pi}_{\mathbf{k}}^\eta = \frac{1}{2} [(\Pi_{\mathbf{k}}^\eta)^{-1} - U_{\mathbf{k}}]^{-1}$ and for K/J within the three-band model, keeping $n_d = 1$ and neglecting the interaction of the oxygen electrons with the magnetic background. We clearly observe that a large nearest-neighbor repulsion V_{pp} and a small bandwidth t_{pp} enhance K . Note that while phonon modes in the same channel are, by symmetry, allowed to give rise to similar behavior, the electronic mechanism for biquadratic exchange is expected to be quantitatively much stronger.

Enhanced nematic susceptibility. The implications of H_K to the physics of underdoped cuprates can be better understood in the limit of $K \gg J$. In this case, the AFM ground state is no longer the Néel configuration with ordering vector $\mathbf{Q} = (\pi, \pi)$, but the striped configuration with $\mathbf{Q} = (\pi, 0)$ or $(0, \pi)$ that is observed in many iron-based superconductors. While the limit of large K/J is clearly not realized in the cuprates, it reveals that H_K supports quantum and classical fluctuations with local striped-magnetic order that have significant statistical weight.

We demonstrate this in Fig. 1(c) by showing typical spin configurations of a Monte Carlo analysis of H_{t-J-K} in the limit of classical spins and where the kinetic energy of the holes is ignored. One clearly sees local striped-magnetic fluctuations (light red background) in an environment of Néel ordered spins (yellow background). Configurations with parallel spins along the x -axis and along the y -axis occur with equal probability, hence preserving the tetragonal symmetry of the system. If one, however, weakly disturbs tetragonal symmetry, e.g. by straining one of the axes, this balance is disturbed and one favors striped configurations of one type over the other.

A natural disturbance of the tetragonal symmetry is, of course, provided by the CuO chains or double chains in $\text{YBa}_2\text{Cu}_3\text{O}_{7-\delta}$ and $\text{YBa}_2\text{Cu}_4\text{O}_8$, respectively, or by external strain [31].

The behavior described above can be quantified in terms of the composite spin variable:

$$\varphi_i = \mathbf{S}_i \cdot (\mathbf{S}_{i-\hat{x}} + \mathbf{S}_{i+\hat{x}} - \mathbf{S}_{i-\hat{y}} - \mathbf{S}_{i+\hat{y}}) \quad (4)$$

which changes sign under a rotation by $\pi/2$. Note that the square of this term, which appears in Eq. (1), is invariant under this transformation, and therefore is fully consistent with the four-fold symmetry of the CuO_2 -plane. While $\langle \varphi_i \rangle = 0$ for realistic values of K (and in the absence of external strain), the static nematic susceptibility

$$\chi_{\text{nem}}(T) = \int_0^{1/T} d\tau \sum_i \langle \mathcal{T}_\tau \varphi_i(\tau) \varphi_0(0) \rangle \quad (5)$$

is a natural measure for the increased relevance of local stripe magnetic configurations. Here, \mathcal{T}_τ denotes imaginary time ordering. In Fig. 2(b-c), we show classical Monte Carlo results for χ_{nem} for a collection of classical Heisenberg spins that interact according to the H_{J-K} model with an additional small second-neighbor exchange $J_2 = -0.1J$ to obtain consistency with the known spin-wave spectrum. One clearly sees that the biquadratic term K enhances the nematic response in the B_{1g} ($x^2 - y^2$) channel, corresponding to an inequivalence between the x and y axes. Most importantly, the nematic susceptibility $\chi_{\text{nem}}(T)$ is non-monotonic, peaking at a temperature governed by the effective exchange interaction of the Cu-spins, $T_{\text{nem}} \sim J$, which is independent on K .

The Monte Carlo results also display that $\chi_{\text{nem}}(T \rightarrow 0) \rightarrow 0$, which is a consequence of the classical nature of the spins in the simulations. As shown in Fig. 3, quantum fluctuations crucially modify this behavior and lead to $\chi_{\text{nem}}(T \rightarrow 0) > 0$. We include the effect of quantum fluctuations by analytically deriving the nematic response within the limit of a large number of (quantum) spin components N . The large- N analysis uses a soft-spin version of the spin degrees of freedom in Eq. (1). After decoupling the biquadratic exchange term K in the nematic channel and taking the long wavelength limit, which is appropriate to study the low-energy excitations, we obtain the effective action:

$$S = S_{\text{dyn}} + \int_r \left[(\nabla \mathbf{n}_r)^2 - \varphi_r \left((\partial_x \mathbf{n}_r)^2 - (\partial_y \mathbf{n}_r)^2 \right) \right] + \int_r \left[r_0 \mathbf{n}_r^2 + \frac{u}{2} (\mathbf{n}_r \cdot \mathbf{n}_r)^2 + \frac{\varphi_r^2}{2g} - h_r \varphi_r \right] \quad (6)$$

where $g \propto K/J > 0$, $u > g$, $\int_r \equiv \int_0^{1/T} d\tau \int d^2r$ and $r = (\tau, \mathbf{r})$ combines imaginary time τ and position $\mathbf{r} = (x, y)$. In addition, φ_r is the nematic order parameter of

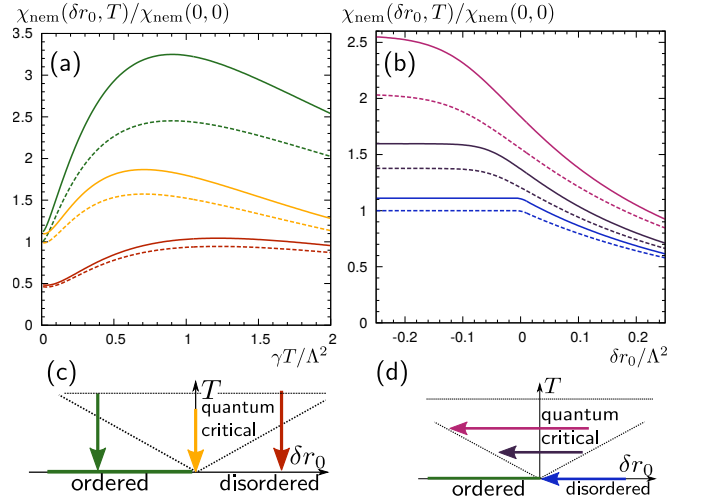


FIG. 3. Nematic susceptibility including quantum fluctuations. Quantum fluctuation effects are included in the analytical large- N treatment of the two-dimensional model. Dashed (solid) lines are for $g = 0$ ($g = 0.1$), where $g \propto K/J$. Panel (a) is for fixed distances to the AFM quantum critical point $\delta r_0 = \{-r_{0,c}, 0, r_{0,c}\}$ (green, yellow, red; see panel (c)) and varying temperature. Note that quantum fluctuations render the susceptibility at $T = 0$ finite, but do not strongly affect the finite temperature behavior. Non-zero g enhances the finite temperature nematic response and increases the maximal value of χ_{nem} around $T \sim \Lambda^2/\gamma \sim J$ (with momentum cutoff $\Lambda = 10$ and frequency cutoff $\gamma\Lambda_\omega = 100$). Panel (b) is for fixed temperatures $T/\Lambda^2 = \{0, 0.1, 0.2\}$ (blue, purple, magenta; see panel (d)) and varying δr_0 . It demonstrates that the nematic response increases with the magnetic correlation length, as the system approaches the quantum critical point. The quartic coefficient is set to $u/\gamma = 50$ in (a) and $u/\gamma = 5$ in (b).

Eq. (4), h_r is an external strain field, and \mathbf{n}_r is the $N = 3$ component staggered Néel order parameter, as used in the non-linear sigma model description of the cuprates in Refs. [42, 44]. The quantum dynamics of the Néel order parameter is governed by $S_{\text{dyn}} = \int_q f(\omega_n) \mathbf{n}_q \cdot \mathbf{n}_{-q}$, where $f(\omega_n) \propto \omega_n^2$ at half filling, while $f(\omega_n) = \gamma|\omega_n|$ was proposed to describe particle-hole excitations. Here, $q = (\omega_n, \mathbf{q})$ combines Matsubara frequency ω_n and momentum \mathbf{q} (measured relative to the AFM ordering vector $\mathbf{Q} = (\pi, \pi)$) and $\int_q \equiv T \sum_n \int \frac{d^2q}{(2\pi)^2}$. The parameter r_0 measures the distance to the AFM quantum critical point, located at $r_{0,c}$. For $\delta r_0 \equiv r_0 - r_{0,c} < 0$, the system has long-range AFM order at $T = 0$, whereas for $\delta r_0 > 0$ it is in the paramagnetic phase (see Fig. 3(c-d)).

In order to make analytic progress we consider the limit where \mathbf{n}_r is an N -component vector and take the limit of large N . This approach led to important insights in both the description of antiferromagnetic correlations of the cuprate parent compounds [44] and of nematic fluctuations of iron-based superconductors [45]. Computing

the nematic susceptibility yields (see [41]):

$$\chi_{\text{nem}} = \frac{\chi_{\text{nem}}^{(0)}}{1 - \frac{g}{N}\chi_{\text{nem}}^{(0)}}, \quad (7)$$

where the bare nematic susceptibility is given by $\chi_{\text{nem}}^{(0)} = \frac{N}{2} \int_{\mathbf{q}} \frac{|\mathbf{q}|^4 \cos^2(2\theta)}{(\xi^{-2} + |\mathbf{q}|^2 + f(\omega_n))^2}$ with $\mathbf{q} = |\mathbf{q}|(\cos \theta, \sin \theta)$. Here, ξ is the magnetic correlation length for Néel order, which is also determined self-consistently within large- N for a given distance to the AFM quantum critical point, δr_0 . Despite the similarity between Eq. (7) and the expression for the nematic susceptibility of iron-based superconductors [45], there are very important differences between the two systems. Because the iron pnictides order magnetically in a striped configuration, $\chi_{\text{nem}}^{(0)}$ diverges when $\xi \rightarrow \infty$, which guarantees that a nematic transition takes place already in the paramagnetic state for any $g > 0$. However, because the cuprates order in a Néel configuration, $\chi_{\text{nem}}^{(0)}$ remains finite even when $\xi \rightarrow \infty$. Although long-range nematic order is not present, nematic fluctuations can be significantly enhanced if the biquadratic exchange $K \propto g$ is sufficiently large.

In Fig. 3 we show the nematic susceptibility obtained within the large- N approach [41]. Like in the Monte Carlo results (see Fig. 2), we observe a broad maximum at finite temperatures around $T \approx J$ (the lattice cutoff Λ plays the role of J in the continuum model). This pronounced peak of χ_{nem} is determined by $\chi_{\text{nem}}^{(0)}$, which in turn is governed by the magnetic correlation length ξ that is set by T/J . The effect of g , and thus of the biquadratic exchange K , is to determine the amplitude of the peak. At low temperatures, we find that in contrast to the results of the classical Monte Carlo simulation, quantum fluctuations render χ_{nem} finite, which is shown in Fig. 3(b). We further observe that the nematic response increases for an increasing magnetic correlation length, i.e. Néel fluctuations enhance the nematic susceptibility, since $\chi_{\text{nem}}(\delta r_0, T)$ is an increasing function for decreasing δr_0 . Note that χ_{nem} is a non-universal quantity whose precise shape depends on microscopic details (such as the lattice constant) and will be different for different materials.

Consequences of long-range nematic order. An immediate consequence of this enhanced nematic susceptibility is that a small tetragonal-symmetry breaking field h , caused either by external strain or by the presence of CuO chains, can induce a sizable nematic order parameter $\varphi \approx \chi_{\text{nem}} h$. From the action in Eq. (6), we can readily obtain the dynamic spin susceptibility in the presence of this induced nematic order

$$\chi_{\text{AFM}}(\mathbf{Q} + \mathbf{q}, \omega) = \frac{1}{\xi^{-2} + \mathbf{q}^2 - \varphi(q_x^2 - q_y^2) + f(\omega_n)}, \quad (8)$$

Therefore, as shown in Fig. 4, non-zero φ modifies the

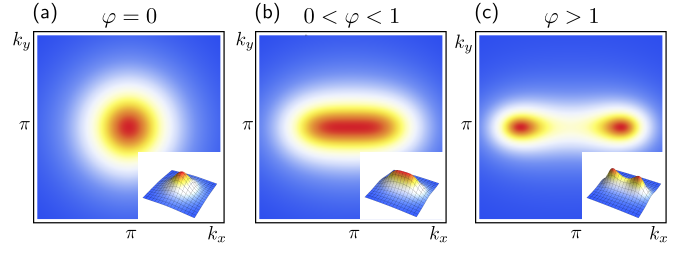


FIG. 4. Incommensurate transition induced by nematic order. Panels (a-c) schematically illustrate the effect of finite nematic order φ on the inelastic neutron scattering cross-section. It shows $\chi_{\text{AFM}}(\mathbf{k})$ from Eq. (8) (including a fourth order term $\propto \mathbf{q}^4$) for $\xi^{-2} = 0.2$ and $\varphi = \{0, 1, 1.5\}$. In the absence of nematic order ($\varphi = 0$) the scattering peak is isotropic around the Néel ordering vector $\mathbf{Q} = (\pi, \pi)$, but non-zero $0 < \varphi < 1$ leads to an elliptic deformation of the peak as observed experimentally [34]. For larger values of $\varphi > 1$ the peak splits and two incommensurate scattering peaks emerge at $(\pi \pm \delta, \pi)$. Note that the inequivalence of x and y direction appears in response to an external (or intrinsic) strain field that explicitly breaks C_4 symmetry.

spin-spin structure factor near the Néel ordering vector \mathbf{Q} from a circular shape, which preserves tetragonal symmetry, to an elliptical shape, which breaks tetragonal symmetry. In addition, as φ increases, it can naturally shift the maximum of $\chi_{\text{AFM}}(\mathbf{Q} + \mathbf{q}, \omega)$ from the commensurate $\mathbf{q} = 0$ value to an incommensurate $\mathbf{q}_{\text{IC}} \neq 0$ value, with \mathbf{q}_{IC} parallel to either the x axis (if $\varphi > 0$) or to the y axis (if $\varphi < 0$). Interestingly, both features – the elliptical structure factor and an anisotropic incommensurate peak – have been observed in YBCO by neutron scattering experiments [8, 34]. In agreement with our model, these effects onset at a temperature scale comparable to the Néel transition temperature in underdoped compositions. Furthermore, Ref. [36] has shown that scattering of itinerant carriers by these anisotropic spin fluctuations cause an anisotropy in the resistivity anisotropy that is consistent with the transport data in YBCO in the same region of the phase diagram [7]. Note that a somewhat related mechanism for the incommensurate spin order, based on the $t - J$ model, was reported in Refs. [46, 47, 49]. Previous works have also focused on nematicity arising from a pre-existing incommensurability [48], whereas in our scenario incommensurate magnetic order is a consequence of nematic order.

While these effects onset in the paramagnetic phase, the presence of nematic order is also manifested in the Néel ordered state by the direction of the Cu moments, which align parallel to either the x axis or to the y axis [35]. Within our model, this observation can be rationalized by invoking the spin-orbit coupling in the oxygen sites, which convert an imbalance in the charge of the $2p_x$ and $2p_y$ orbitals into a preferred direction for the Cu moment.

At first sight, one might anticipate that K would af-

fect the spin-wave dispersion, which, experimentally, is well described in terms of J and a small ferromagnetic nearest-neighbor exchange J_2 only [50]. As we show in the SM [41], however, the biquadratic exchange of Eq. (1) does not modify the linearized spin-wave spectrum. The reason for this peculiar behavior is that the biquadratic exchange annihilates the classical Néel state, i.e. the vacuum of the linear spin wave excitations:

$$H_K |\text{Néel}\rangle = 0. \quad (9)$$

Thus, while it seems impossible to gain insight about the biquadratic exchange from measurements of the spin wave dispersion, it is also true that such measurements are fully consistent with the new Hamiltonian Eq. (1).

Comparison with experiments and conclusions. In summary, we showed that charge fluctuations associated with hole-doping in the oxygen orbitals generate a biquadratic exchange coupling between the Cu spins, extending the celebrated $t - J$ model employed to describe lightly-doped cuprates. The main effect of this biquadratic term is to enhance B_{1g} nematic fluctuations, which however is not translated into a diverging nematic susceptibility. Most importantly, the temperature in which the nematic susceptibility peaks is determined not by the biquadratic coupling K , but by the standard nearest-neighbor exchange coupling J . The amplitude of the peak, however, is controlled by K , which increases for larger values of V_{pp} .

These results are consistent with the current experimental scenario: first, nematic order seems to be observed only in hole-doped compounds whose lattice structures explicitly break tetragonal symmetry [12, 13]. Within our model, such a small symmetry-breaking field takes advantage of the large (but non-diverging) nematic susceptibility and induces nematic order. Second, the observed temperature scale for the onset of the induced nematic order is comparable to the Néel transition temperature, which in turn is set by J [8, 34]. Third, our model naturally addresses the main manifestations of the induced nematic order observed experimentally in the spin spectrum – the elliptical spin-spin structure factor, the anisotropic incommensurate AFM peak, and the direction of the Cu moments inside the AFM state [8, 34, 35].

To further verify the validity of our scenario, it would be desirable to directly measure the nematic susceptibility in cuprates. Our main result is the non-monotonic temperature dependence of χ_{nem} , with a peak at $T \sim J$. In analogy to what has been done for the iron-pnictides (see Ref. [51]), χ_{nem} is closely related to several observables, such as the elastoresistance, the shear modulus, or electronic Raman scattering. According to our model, performing these measurements in underdoped tetragonal systems, such as $\text{HgBa}_2\text{CuO}_4$, should reveal an enhanced nematic response without long-range order. Similarly, we predict this behavior to be much weaker in tetragonal electron-doped systems, such as Nd_2CuO_4 ,

where oxygen charge fluctuations are expected to be less relevant, since electron-doping involves Cu orbitals.

Finally, an interesting open question is the effect of such enhanced nematic fluctuations on the superconducting state. In particular, the close connection between nematic and Néel spin fluctuations offers an interesting scenario to investigate the formation of Cooper pairs. Indeed, recent theoretical studies have revealed that nematic fluctuations, in conjunction with another pairing mechanism, may provide a sizable boost to the superconducting transition temperature [52].

We gratefully acknowledge helpful discussions with A. Chubukov, B. Keimer and M. Le Tacon. P.P.O. acknowledges support from Iowa State University Startup Funds. J.S. acknowledges financial support by the Deutsche Forschungsgemeinschaft through Grant No. SCHM 1031/7-1. This work was carried out using the computational resource bwUniCluster funded by the Ministry of Science, Research and Arts and the Universities of the State of Baden-Württemberg, Germany, within the framework program bwHPC.

-
- [1] B. Keimer, S. A. Kivelson, M. R. Norman, S. Uchida, and J. Zaanen, *Nature* **518**, 179 (2015).
 - [2] E. Fradkin, S. A. Kivelson, and J. M. Tranquada, *Rev. Mod. Phys.* **87**, 457 (2015).
 - [3] T. Wu, H. Mayaffre, S. Kramer, M. Horvatic, C. Berthier, W. N. Hardy, R. Liang, D. A. Bonn, and M.-H. Julien, *Nature* **477**, 191 (2011).
 - [4] G. Ghiringhelli, M. Le Tacon, M. Minola, S. Blanco-Canosa, C. Mazzoli, N. B. Brookes, G. M. De Luca, A. Frano, D. G. Hawthorn, F. He, T. Loew, M. Moretti Sala, D. C. Peets, M. Salluzzo, E. Schierle, R. Sutarto, G. A. Sawatzky, E. Weschke, B. Keimer, and L. Braicovich, *Science* **337**, 821 (2012).
 - [5] J. Chang, E. Blackburn, A. T. Holmes, N. B. Christensen, J. Larsen, J. Mesot, R. Liang, D. A. Bonn, W. N. Hardy, A. Watenphul, M. v. Zimmermann, E. M. Forgan, and S. M. Hayden, *Nat. Phys.* **8**, 871 (2012).
 - [6] D. LeBoeuf, S. Krämer, W. N. Hardy, R. Liang, D. A. Bonn, and C. Proust, *Nat. Phys.* **9**, 79 (2013).
 - [7] Y. Ando, K. Segawa, S. Komiya, and A. N. Lavrov, *Phys. Rev. Lett.* **88**, 137005 (2002).
 - [8] V. Hinkov, D. Haug, B. Fauqué, P. Bourges, Y. Sidis, A. Ivanov, C. Bernhard, C. T. Lin, and B. Keimer, *Science* **319**, 597 (2008).
 - [9] R. Daou, J. Chang, D. LeBoeuf, O. Cyr-Choiniere, F. Laliberte, N. Doiron-Leyraud, B. J. Ramshaw, R. Liang, D. A. Bonn, W. N. Hardy, and L. Taillefer, *Nature* **463**, 519 (2010).
 - [10] M. J. Lawler, K. Fujita, L. Jinhwan, A. R. Schmidt, Y. Kohsaka, K. C. Koo, H. Eisaki, S. Uchida, J. C. Davis, J. P. Sethna, and E.-A. Kim, *Nature* **466**, 347 (2010).
 - [11] B. J. Ramshaw, N. Harrison, S. E. Sebastian, S. Ghanad-zadeh, K. A. Modic, D. A. Bonn, W. N. Hardy, R. Liang, and P. A. Goddard, *npj Quantum Materials* **2**, 8 (2017).

- [12] S. A. Kivelson, I. P. Bindloss, E. Fradkin, V. Oganessian, J. M. Tranquada, A. Kapitulnik, and C. Howald, *Rev. Mod. Phys.* **75**, 1201 (2003).
- [13] M. Vojta, *Adv. Phys.* **58**, 699 (2009).
- [14] M. Vilk and A.-M. S. Tremblay, *J. Phys. I (France)* **7**, 1309 (1997).
- [15] A. V. Chubukov and D. K. Morr, *Phys. Rep.* **288**, 355 (1997).
- [16] J. Schmalian, D. Pines, and B. Stojković, *Phys. Rev. Lett.* **80**, 3839 (1998).
- [17] J. Zaanen, G. A. Sawatzky, J. W. Allen, *Phys. Rev. Lett.* **55**, 418 (1985).
- [18] M. K. Chan, C. J. Dorow, L. Mangin-Thro, Y. Tang, Y. Ge, M. J. Veit, G. Yu, X. Zhao, A. D. Christianson, J. T. Park, Y. Sidis, P. Steffens, D. L. Abernathy, P. Bourges, and M. Greven, *Nat. Commun.* **7**, 10819 (2016).
- [19] S. Badoux, W. Tabis, F. Laliberté, G. Grissonnache, B. Vignolle, D. Vignolles, J. Béard, D. A. Bonn, W. N. Hardy, R. Liang, N. Doiron-Leyraud, L. Taillefer, and C. Proust, *Nature* **531**, 210 (2016).
- [20] N. Barišić, M. K. Chan, M. J. Veit, C. J. Dorow, Y. Ge, Y. Tang, W. Tabis, G. Yu, X. Zhao, and M. Greven, *arXiv:1507.07885*.
- [21] K. B. Efetov, H. Meier, and C. Pepin, *Nat. Phys.* **9**, 442 (2013).
- [22] S. Sachdev and R. La Placa, *Phys. Rev. Lett.* **111**, 027202 (2013).
- [23] Y. Wang and A. Chubukov, *Phys. Rev. B* **90**, 035149 (2014).
- [24] S. A. Kivelson, E. Fradkin, and V. J. Emery, *Nature* **393**, 550 (1998).
- [25] P. A. Lee, N. Nagaosa, and X.-G. Wen, *Rev. Mod. Phys.* **78**, 17 (2006).
- [26] S. A. Kivelson, E. Fradkin, and T. H. Geballe, *Phys. Rev. B* **69**, 144505 (2004).
- [27] M. H. Fischer and E.-A. Kim, *Phys. Rev. B* **84**, 144502 (2011).
- [28] S. Bulut, W. A. Atkinson, and A. P. Kampf, *Phys. Rev. B* **88**, 155132 (2013).
- [29] M. H. Fischer, S. Wu, M. Lawler, A. Paramekanti, and E.-A. Kim, *New J. Phys.* **16**, 093057 (2014).
- [30] P. A. Volkov and K. B. Efetov, *Phys. Rev. B* **93**, 085131 (2016).
- [31] J.-H. Chu, H.-H. Kuo, J. G. Analytis, and I. R. Fisher, *Science* **337**, 710 (2012).
- [32] B. M. Andersen, S. Graser, and P. J. Hirschfeld, *Europhys. Lett.* **97**, 47002 (2012).
- [33] S. Okamoto, D. Sénéchal, M. Civelli, and A.-M. Tremblay, *Phys. Rev. B* **82**, 180511(R) (2010).
- [34] D. Haug, V. Hinkov, Y. Sidis, P. Bourges, N. B. Christensen, A. Ivanov, T. Keller, C. T. Lin, and B. Keimer, *New J. Phys.* **12**, 105006 (2010).
- [35] B. Nafradi, T. Keller, F. Hardy, C. Meingast, A. Erb, and B. Keimer, *Phys. Rev. Lett.* **116**, 047001 (2016).
- [36] M. Schütt and R. M. Fernandes, *Phys. Rev. Lett.* **115**, 027005 (2015).
- [37] N. P. Armitage, P. Fournier, and R. L. Greene, *Rev. Mod. Phys.* **82**, 2421 (2010).
- [38] V. J. Emery, *Phys. Rev. Lett.* **58**, 2794 (1987).
- [39] J. Zaanen and A. M. Oles, *Phys. Rev. B* **37**, 9423 (1988).
- [40] E. Kolley, W. Kolley, R. Tietz, *J. Phys. Condens. Matter* **4**, 3517 (1992).
- [41] See Supplemental Material.
- [42] S. Chakravarty, B. I. Halperin, and D. R. Nelson, *Phys. Rev. B* **39**, 2344 (1989).
- [43] M. H. Hamidian, S. D. Edkins, C.-K. Kim, J. C. Davis, A. P. Mackenzie, H. Eisaki, S. Uchida, M. J. Lawler, E.-A. Kim, S. Sachdev, and K. Fujita, *Nat. Phys.* **12**, 150 (2016).
- [44] A. V. Chubukov, S. Sachdev, and J. Ye, *Phys. Rev. B* **49**, 11919 (1994).
- [45] R. M. Fernandes, A. V. Chubukov, J. Knolle, I. Eremin, and J. Schmalian, *Phys. Rev. B* **85**, 024534 (2012).
- [46] B. I. Shraiman and E. D. Siggia, *Phys. Rev. Lett.* **61**, 467 (1998).
- [47] O. P. Sushkov and V. N. Kotov, *Phys. Rev. Lett.* **94**, 097005 (2005).
- [48] L. Nie, A. V. Maharaj, E. Fradkin, and S. A. Kivelson, *arXiv:1701.0275*.
- [49] M. Gabay and P. J. Hirschfeld, *Physica C* **162**, 823 (1989).
- [50] R. Coldea, S. M. Hayden, G. Aeppli, T. G. Perring, C. D. Frost, T. E. Mason, S.-W. Cheong, and Z. Fisk, *Phys. Rev. Lett.* **86**, 5377 (2001).
- [51] R. M. Fernandes, A. V. Chubukov, and J. Schmalian, *Nat. Phys.* **10**, 97 (2014).
- [52] S. Lederer, Y. Schattner, E. Berg, and S. A. Kivelson, *Phys. Rev. Lett.* **114**, 097001 (2015).

Supplemental Material for “Enhanced nematic fluctuations near the Mott insulating phase of high- T_c cuprates”

Peter P. Orth,¹ Bhilahari Jeevanesan,² Rafael M. Fernandes,³ and Jörg Schmalian^{2, 4}

¹*Department of Physics and Astronomy, Iowa State University, Ames, Iowa 50011, USA*

²*Institute for Theory of Condensed Matter, Karlsruhe Institute of Technology (KIT), 76131 Karlsruhe, Germany*

³*School of Physics and Astronomy, University of Minnesota, Minneapolis, Minnesota 55455, USA*

⁴*Institute for Solid State Physics, Karlsruhe Institute of Technology (KIT), 76131 Karlsruhe, Germany*

(Dated: March 5, 2017)

CONTENTS

S1. Derivation of $t - J - K$ model Hamiltonian from three-band Hubbard model	8
S1.A. Strong-coupling expansion	9
S1.B. Derivation of biquadratic spin exchange K_0 from microscopic Hamiltonian	9
S1.C. Analysis of bare biquadratic exchange coupling constant K_0	11
S1.D. Renormalization of biquadratic exchange coupling K by quadrupolar oxygen density fluctuations	13
S2. Nematic susceptibility within a soft-spin description of the half-filled $t - J - K$ -model	13
S2.A. Nematic susceptibility $\chi_{\text{nem},0}(r, T)$	14
S2.B. Large- N analysis of the nematic susceptibility	16
S3. Spin-wave treatment of $t - J - K$ model at half-filling	17
S4. Details on the Monte-Carlo simulations	18
References	18

S1. Derivation of $t - J - K$ model Hamiltonian from three-band Hubbard model

The starting point of a microscopic derivation of the biquadratic spin exchange term in the $t - J - K$ model in Eq. (1) of the main text is the three-band Hubbard model [1]: $H = H_0 + H_U + H_V$ with parts

$$H_0 = \sum_{\mathbf{R}_i, \sigma} \left\{ (\epsilon_p - \epsilon_d) n_{i\sigma}^p + t_{pd} \sum_u \left[(-1)^u d_{i\sigma}^\dagger p_{i+u\sigma} + \text{h.c.} \right] + t_{pp} \sum_{u'} \left[(-1)^{u'} p_{i+\frac{\hat{x}}{2}\sigma}^\dagger p_{i+\frac{\hat{x}}{2}+u'\sigma} + \text{h.c.} \right] \right\} \quad (\text{S.1})$$

$$H_U = \sum_{\mathbf{R}_i} \left(U_{dd} n_{i\uparrow}^d n_{i\downarrow}^d + U_{pp} \sum_{u=\frac{\hat{x}}{2}, \frac{\hat{y}}{2}} n_{i+u\uparrow}^p n_{i+u\downarrow}^p \right) \quad (\text{S.2})$$

$$H_V = \sum_{\mathbf{R}_i} \left(V_{pd} \sum_u n_i^d n_{i+u}^p + V_{pp} \sum_{u'} n_{i+\frac{\hat{x}}{2}}^p n_{i+\frac{\hat{x}}{2}+u'}^p \right). \quad (\text{S.3})$$

Here, $d_{i\sigma}^\dagger$ creates a Cu ($3d_{x^2-y^2}$) hole with spin σ at Bravais lattice site \mathbf{R}_i . The operators $p_{i+\frac{\hat{x}}{2}\sigma}^\dagger$ and $p_{i+\frac{\hat{y}}{2}\sigma}^\dagger$ create O ($2p_x$) and ($2p_y$) holes in the same unit cell \mathbf{R}_i , respectively. The vacuum is defined as filled Cu^+ (d^{10}) and O^{2-} (p^6) states. We define the total number of Cu holes with spin σ in unit cell \mathbf{R}_i as $n_i^d = d_{i\sigma}^\dagger d_{i\sigma}$ and the Cu hole density as $n_i^d = \sum_\sigma n_{i\sigma}^d$. The corresponding operators for oxygen holes read $n_{i\sigma}^p = \sum_{u=\frac{\hat{x}}{2}, \frac{\hat{y}}{2}} p_{i+u\sigma}^\dagger p_{i+u\sigma}$ and $n_i^p = \sum_\sigma n_{i\sigma}^p$.

The on-site energies of $d(p)$ orbitals are denoted $\epsilon_d(\epsilon_p)$ with $\Delta = \epsilon_p - \epsilon_d > 0$. The phase factors in the hopping terms arise from the overlap of orbital wavefunctions (see Fig. 1(b) of the main text) and are given by $(-1)^u = +1$ for $u = -\frac{\hat{x}}{2}, \frac{\hat{y}}{2}$, $(-1)^u = -1$ for $u = \frac{\hat{x}}{2}, -\frac{\hat{y}}{2}$ and $(-1)^{u'} = +1$ for $u' = \pm\frac{1}{2}(\hat{x} + \hat{y})$, $(-1)^{u'} = -1$ for $u' = \pm\frac{1}{2}(\hat{x} - \hat{y})$. The (unrestricted) sum \sum_u runs over the four vectors connecting a central Cu site to its four neighboring O sites $u \in \{\pm\frac{\hat{x}}{2}, \pm\frac{\hat{y}}{2}\}$, and the sum $\sum_{u'}$ runs over the four vectors connecting an O p_x orbital to its four p_y neighbors $u' \in \{\pm\frac{1}{2}(\hat{x} \pm \hat{y})\}$. We consider on-site interactions U_{dd} and U_{pp} on both Cu and O sites as well as nearest-neighbor interactions V_{pd} between Cu and O and V_{pp} between oxygens.

S1.A. Strong-coupling expansion

The hierarchy of energy scales suggests a strong-coupling expansion in small $t_{pd} \ll U_{dd} - \Delta, \Delta$, which yields a description in terms of localized Cu spins coupled to mobile O holes. Note that in order to derive the biquadratic exchange interaction term $\propto K$ in Eq. (1) of the main text, one can focus on the case of singly occupied Cu sites, *i.e.*, all holes reside on the oxygen sites. In the strong coupling expansion we follow Ref. 2 (see also Ref. 3) that contains an expansion up to fourth order in $t_{pd}^4/[\Delta^n(U_{dd} - \Delta)^m]$ with $n + m = 3$ within this subspace. At second order one finds a term that renormalizes t_{pp} and a Cu-O Kondo like exchange coupling term

$$H_{dp}^{(2)} = 2t_{pd}^2 \left(\frac{1}{\Delta} + \frac{1}{U - \Delta} \right) \sum_{i, u_1, u_2} (-1)^{u_1+u_2} \mathbf{s}_{i+u_1, i+u_2} \cdot \mathbf{S}_i \quad (\text{S.4})$$

with (non-)local O spin operators $\mathbf{s}_{ij} = \frac{1}{2} \sum_{\tau, \tau'} p_{i\tau}^\dagger \boldsymbol{\sigma}_{\tau\tau'} p_{j\tau'}$ with $\boldsymbol{\sigma} = (\sigma^x, \sigma^y, \sigma^z)$ being a vector of Pauli matrices and Cu spin operators $\mathbf{S}_i = \frac{1}{2} \sum_{\tau, \tau'} d_{i\tau}^\dagger \boldsymbol{\sigma}_{\tau\tau'} d_{i\tau}$. At fourth order, there appear further Cu-O Kondo-like exchange terms, the well-known Heisenberg Cu-Cu spin exchange term

$$H_J^{(4)} = J \sum_{\langle i, j \rangle} \mathbf{S}_i \cdot \mathbf{S}_j \quad (\text{S.5})$$

with $J = t_{pd}^4 \left(\frac{2}{\Delta^3} + \frac{3}{2\Delta^2(U_{dd} - \Delta)} - \frac{1}{2\Delta(U_{dd} - \Delta)^2} \right)$ and a term that renormalizes hopping and interactions among oxygen sites. Most importantly for our analysis, however, there also appears a Cu spin exchange term that depends on the hole occupation number of the intermediate O orbital

$$H_{J'} = -J' \sum_{i, \delta} n_{i+\frac{\delta}{2}}^p \mathbf{S}_i \cdot \mathbf{S}_{i+\delta} \quad (\text{S.6})$$

with $J' = t_{pd}^4 \left(\frac{1}{\Delta^3} + \frac{1}{\Delta^2(U_{dd} - \Delta)} - \frac{1}{\Delta(U_{dd} - \Delta)^2} - \frac{1}{(U_{dd} - \Delta)^3} \right)$ and $\delta = \{\pm\hat{x}, \pm\hat{y}\}$. After integration of oxygen density fluctuation, this term will give rise to the biquadratic spin exchange as we show below. Note that in the limit of large- U_{dd} , one finds $\lim_{U_{dd} \rightarrow \infty} J'/J = 1/2$, so this term is of the same order as the Heisenberg spin-exchange.

There also appear non-local manifestations of this term with n_i^p being replaced by $n_{ij}^p = \sum_{\sigma} p_{i\sigma}^\dagger p_{j\sigma}$ and term that describes coupling of the (non-)local spin density on the intermediate oxygen site to the cross product of Cu spins $H_{ddp}^{(4)} \propto [-2i \sum_{\langle i, j \rangle, u_1, u_2} \mathbf{s}_{i+u_1, j+u_2} \cdot (\mathbf{S}_i \times \mathbf{S}_j)]$, which are, however, not the focus of our analysis.

S1.B. Derivation of biquadratic spin exchange K_0 from microscopic Hamiltonian

To consider the effect of charge fluctuations on the oxygen sites, we rewrite the oxygen interaction part of the Hamiltonian $H_{U_{pp}} + H_{V_{pp}}$ in terms of total n_i^p and relative oxygen density η_i within unit cell \mathbf{R}_i :

$$n_i^p = n_{i+\frac{\hat{x}}{2}}^p + n_{i+\frac{\hat{y}}{2}}^p \quad (\text{S.7})$$

$$\eta_i = n_{i+\frac{\hat{x}}{2}}^p - n_{i+\frac{\hat{y}}{2}}^p. \quad (\text{S.8})$$

This allows to write the oxygen-density-dependent interaction between neighboring Cu spins in Eq. (S.6) as

$$H_{J'} = -\frac{J'}{2} \sum_i \left[\eta_i (\mathbf{S}_i \cdot \mathbf{S}_{i+\hat{x}} - \mathbf{S}_i \cdot \mathbf{S}_{i+\hat{y}}) + \eta_{i-\hat{x}} \mathbf{S}_i \cdot \mathbf{S}_{i-\hat{x}} - \eta_{i-\hat{y}} \mathbf{S}_i \cdot \mathbf{S}_{i-\hat{y}} + n_i^p (\mathbf{S}_i \cdot \mathbf{S}_{i+\hat{x}} + \mathbf{S}_i \cdot \mathbf{S}_{i+\hat{y}}) + \sum_{\delta=\hat{x}, \hat{y}} n_{i-\delta}^p \mathbf{S}_i \cdot \mathbf{S}_{i-\delta} \right] \quad (\text{S.9})$$

The on-site (U_{pp}) and nearest-neighbor (V_{pp}, V_{pd}) oxygen interaction terms in Eq. (S.2) and (S.3) take the form

$$H_{U_{pp}} + H_{V_{pp}} + H_{V_{pd}} = \frac{1}{N_L} \sum_{\mathbf{k}} \left[U_{+, \mathbf{k}} n_{\mathbf{k}}^p n_{-\mathbf{k}}^p - U_{-, \mathbf{k}} \eta_{\mathbf{k}} \eta_{-\mathbf{k}} + \frac{V_{pp} f_{\mathbf{k}}}{4} (\eta_{\mathbf{k}} n_{-\mathbf{k}}^p - \eta_{-\mathbf{k}} n_{\mathbf{k}}^p) \right] + 2V_{pd} n_0^p \quad (\text{S.10})$$

where we introduce the interactions $U_{\pm, \mathbf{k}} = \frac{V_{pp} f_{\mathbf{k}}}{4} \pm \frac{U_{pp}}{8}$ and we write the Fourier transform as $\eta_i = \frac{1}{N_L} \sum_{\mathbf{k}} \eta_{\mathbf{k}} e^{i\mathbf{k} \cdot \mathbf{R}_i}$ with total number of unit cells N_L . The lattice function is given by $f_{\mathbf{k}} = \sum_{\delta'} e^{-i\mathbf{k} \cdot \delta'} = 1 + e^{-ik_x} + e^{ik_y} + e^{i(k_y - k_x)}$.

Here, $\delta' \in \{0, \hat{x}, -\hat{y}, \hat{x} - \hat{y}\}$ denotes Bravais lattice vectors pointing to unit cells containing the four nearest-neighbor p_y oxygen orbitals of a given oxygen p_x orbital.

As required, Eq. (S.10) is invariant under the spatial symmetries of the system. In particular, it is invariant under fourfold C_4 rotation $C_4(x_i, y_i) = (-y_i, x_i)$, $C_4(k_x, k_y) = (-k_y, k_x)$. This follows from the transformation laws of the orbitals $p_{i+\frac{\hat{x}}{2}} \xrightarrow{C_4} p_{C_4(i)+\frac{\hat{y}}{2}}$ and $p_{i+\frac{\hat{y}}{2}} \xrightarrow{C_4} p_{C_4(i)-\frac{\hat{x}}{2}}$. The transformation laws for total and relative densities follow as $\eta_{\mathbf{k}} \xrightarrow{C_4} \frac{1}{2}(1 - e^{-ik_x})n_{\mathbf{k}}^p - \frac{1}{2}(1 + e^{-ik_x})\eta_{\mathbf{k}}$ and $n_{\mathbf{k}}^p \xrightarrow{C_4} \frac{1}{2}(1 + e^{-ik_x})n_{\mathbf{k}}^p + \frac{1}{2}(e^{-ik_x} - 1)\eta_{\mathbf{k}}$. Noting that $f_{\mathbf{k}} \xrightarrow{C_4} f_{C_4^{-1}(\mathbf{k})} = 1 + e^{-ik_y} + e^{-ik_x} + e^{-i(k_y+k_x)} = e^{-ik_y}f_{\mathbf{k}}$, one can easily show using $e^{i(k_x-k_y)}f_{\mathbf{k}} = f_{-\mathbf{k}}$ that Eq. (S.10) is invariant under C_4 rotations.

Since the operators $\eta_{\mathbf{k}}$ and $n_{\mathbf{k}}^p$ transform into each other under symmetry transformations (such as C_4), we need to treat them on equal footing when decoupling the interaction terms using a Hubbard-Stratonovich (HS) transformation. We introduce the vector $v_{\mathbf{k}} = (n_{\mathbf{k}}^p, \eta_{\mathbf{k}})^T$ and write $H_{U_{pp}} + H_{V_{pp}} = -\sum_{\mathbf{k}, k_x > 0} v_{\mathbf{k}}^\dagger U_{\mathbf{k}}^{-1} v_{\mathbf{k}}$ with interaction matrix

$$U_{\mathbf{k}}^{-1} = \frac{2}{N_L} \begin{pmatrix} -\text{Re } U_{+, \mathbf{k}} & i \frac{V_{pp}}{4} \text{Im } f_{\mathbf{k}} \\ -i \frac{V_{pp}}{4} \text{Im } f_{\mathbf{k}} & \text{Re } U_{-, \mathbf{k}} \end{pmatrix} \rightarrow U_{\mathbf{k}} = \frac{N_L}{2} \frac{1}{\left(\frac{V_{pp}}{4}\right)^2 |f_{\mathbf{k}}|^2 + \left(\frac{U_{pp}}{8}\right)^2} \begin{pmatrix} -\text{Re } U_{-, \mathbf{k}} & i \frac{V_{pp}}{4} \text{Im } f_{\mathbf{k}} \\ -i \frac{V_{pp}}{4} \text{Im } f_{\mathbf{k}} & \text{Re } U_{+, \mathbf{k}} \end{pmatrix}. \quad (\text{S.11})$$

The HS transformation introduces the fields $\Phi_{\mathbf{k}} = (\psi_{\mathbf{k}}, \phi_{\mathbf{k}})$ and yields the action

$$S_{U_{pp}+V_{pp}} = \int_{\mathbf{k}} (\Phi_{\mathbf{k}}^\dagger U_{\mathbf{k}} \Phi_{\mathbf{k}} - \Phi_{\mathbf{k}}^\dagger v_{\mathbf{k}} - v_{\mathbf{k}}^\dagger \Phi_{\mathbf{k}}), \quad (\text{S.12})$$

where $k = (ik_n, \mathbf{k})$ combines Matsubara frequency $ik_n = 2\pi nT$ with temperature T and momentum \mathbf{k} . We note that the fields $\Phi_{\mathbf{k}}$ transform identical to $v_{\mathbf{k}}$ in order that the action remains invariant under all symmetry transformations.

We have arrived at an action that is quadratic in oxygen hole operators. In a next step, we will perform the exact functional integration over these degrees of freedom. We focus on those terms in the action that are relevant for the derivation of the biquadratic exchange interaction $S = S_0 + S_{U_{pp}+V_{pp}} + S_{J'}$, which read explicitly

$$S = - \int_{q, k} \sum_{u, u', \sigma, \sigma'} p_{qu\sigma}^\dagger G_{qu\sigma, ku'\sigma'}^{-1} p_{ku'\sigma'} + \int_{\mathbf{k}} \Phi_{\mathbf{k}}^\dagger U_{\mathbf{k}} \Phi_{\mathbf{k}}, \quad (\text{S.13})$$

where $u, u' \in \{x, y\}$ label (p_x, p_y) orbitals and $\sigma, \sigma' \in \{\uparrow, \downarrow\}$ denote the spin direction. The inverse Green's function $G^{-1}(\mathbf{S}_i)$ in Eq. (S.13) contains the Cu spin operators \mathbf{S}_i and is a sum of terms

$$G^{-1} = G_0^{-1} + G_{U_{pp}+V_{pp}}^{-1} + G_{J'}^{-1} \quad (\text{S.14})$$

Since all Green's functions are diagonal in spin space, $G^{-1} \propto \sigma^0$ with $\sigma^0 = \text{diag}(1, 1)$, we suppress the spin indices in the following and find

$$G_{0;qu,qu'}^{-1} = (iq_n - \Delta + \mu - 2V_{pd})\tau^0 - t_{pp}\text{Re}(h_{\mathbf{q}})\tau^x + t_{pp}\text{Im}(h_{\mathbf{q}})\tau^y \quad (\text{S.15})$$

$$G_{U_{pp}+V_{pp};qu,ku'}^{-1} + G_{J';qu,ku'}^{-1} = a_{0,q-k}\tau^0 + a_{z,q-k}\tau^z. \quad (\text{S.16})$$

Here, τ^α are Pauli matrices in orbital (p_x, p_y) space, $\tau^0 = \text{diag}(1, 1)$ and we have defined the lattice function

$$h_{\mathbf{q}} = 1 - e^{iq_x} - e^{-iq_y} + e^{i(q_x - q_y)} \quad (\text{S.17})$$

that describes oxygen hopping. We have also introduced the functions

$$a_{0,q-k} = \psi_{q-k} - \sum_{\mathbf{p}} \mathcal{S}_{\mathbf{p}, \mathbf{q}-\mathbf{k}} h_m(\mathbf{p}, \mathbf{k}-\mathbf{q}) \quad (\text{S.18})$$

$$a_{z,q-k} = \phi_{q-k} - \sum_{\mathbf{p}} \mathcal{S}_{\mathbf{p}, \mathbf{q}-\mathbf{k}} h_\eta(\mathbf{p}, \mathbf{k}-\mathbf{q}). \quad (\text{S.19})$$

These functions contain the HS fields $\psi_{\mathbf{k}}$ and $\phi_{\mathbf{k}}$ as well as the spin bilinear $\mathcal{S}_{\mathbf{p}, \mathbf{q}} = \mathbf{S}_{\mathbf{p}} \cdot \mathbf{S}_{-\mathbf{p}-\mathbf{q}}$. Under a C_4 rotation it remains invariant $C_4(\mathcal{S}_{\mathbf{p}, \mathbf{q}}) = \mathcal{S}_{\mathbf{p}, \mathbf{q}}$. The interaction of Cu spins with the intermediate oxygen site [see Eq. (S.9)] is captured in Fourier space by the lattice functions

$$h_m(\mathbf{p}, \mathbf{k}) = \frac{J'}{2} (e^{ip_x} + e^{ip_y} + e^{-i(p_x+k_x)} + e^{-i(p_y+k_y)}) \quad (\text{S.20})$$

$$h_\eta(\mathbf{p}, \mathbf{k}) = \frac{J'}{2} (e^{ip_x} - e^{ip_y} + e^{-i(p_x+k_x)} - e^{-i(p_y+k_y)}). \quad (\text{S.21})$$

Functional integration over $p_{qu\sigma}^\dagger$ and $p_{qu\sigma}$ yields the action

$$S = \int_k \Phi_k^\dagger U_k \Phi_k - \text{Tr} \log(-G^{-1}) = \int_k \Phi_k^\dagger U_k \Phi_k + \frac{1}{2} \text{Tr}[\{G_0(G_{U_{pp}+V_{pp}}^{-1} + G_{J'}^{-1})\}^2] + \dots \quad (\text{S.22})$$

where the ellipsis stands for the zeroth, first and higher order terms. Focusing on the quadratic term, we write it as

$$S_2 = \frac{1}{2} \text{Tr}[\{G_0(G_{U_{pp}+V_{pp}}^{-1} + G_{J'}^{-1})\}^2] = -\frac{1}{2} \int_q \sum_{\alpha, \beta \in \{0, z\}} a_{\alpha, q} a_{\beta, -q} \Pi_{-q}^{\alpha\beta}, \quad (\text{S.23})$$

where we have introduced the response functions

$$\Pi_q^{\alpha\beta} = - \int_k \text{Tr}[G_{0, k}(\tau^\alpha \sigma^0) G_{0, k+q}(\tau^\beta \sigma^0)]. \quad (\text{S.24})$$

Performing the summation over Matsubara frequencies and setting the external frequency iq_n to zero, they read

$$\Pi_q^{00} = \int_k \frac{2}{\epsilon_{\mathbf{k}+\mathbf{q}}^2 - \epsilon_{\mathbf{k}}^2} \left\{ \frac{\epsilon_{\mathbf{k}}^2 + g_{+, \mathbf{k}, \mathbf{q}}}{\epsilon_{\mathbf{k}}} [n_F(\tilde{\Delta} + \epsilon_{\mathbf{k}}) - n_F(\tilde{\Delta} - \epsilon_{\mathbf{k}})] - \frac{\epsilon_{\mathbf{k}+\mathbf{q}}^2 + g_{+, \mathbf{k}, \mathbf{q}}}{\epsilon_{\mathbf{k}+\mathbf{q}}} [n_F(\tilde{\Delta} + \epsilon_{\mathbf{k}+\mathbf{q}}) - n_F(\tilde{\Delta} - \epsilon_{\mathbf{k}+\mathbf{q}})] \right\} \quad (\text{S.25})$$

$$\Pi_q^{z0} = \int_k \frac{2g_{-, \mathbf{k}, \mathbf{q}}}{\epsilon_{\mathbf{k}+\mathbf{q}}^2 - \epsilon_{\mathbf{k}}^2} \left\{ \frac{n_F(\tilde{\Delta} + \epsilon_{\mathbf{k}}) - n_F(\tilde{\Delta} - \epsilon_{\mathbf{k}})}{\epsilon_{\mathbf{k}}} - \frac{n_F(\tilde{\Delta} - \epsilon_{\mathbf{k}+\mathbf{q}}) - n_F(\tilde{\Delta} - \epsilon_{\mathbf{k}+\mathbf{q}})}{\epsilon_{\mathbf{k}+\mathbf{q}}} \right\} \quad (\text{S.26})$$

$$\Pi_q^{zz} = \int_k \frac{2}{\epsilon_{\mathbf{k}+\mathbf{q}}^2 - \epsilon_{\mathbf{k}}^2} \left\{ \frac{\epsilon_{\mathbf{k}}^2 - g_{+, \mathbf{k}, \mathbf{q}}}{\epsilon_{\mathbf{k}}} [n_F(\tilde{\Delta} + \epsilon_{\mathbf{k}}) - n_F(\tilde{\Delta} - \epsilon_{\mathbf{k}})] - \frac{\epsilon_{\mathbf{k}+\mathbf{q}}^2 - g_{+, \mathbf{k}, \mathbf{q}}}{\epsilon_{\mathbf{k}+\mathbf{q}}} [n_F(\tilde{\Delta} + \epsilon_{\mathbf{k}+\mathbf{q}}) - n_F(\tilde{\Delta} - \epsilon_{\mathbf{k}+\mathbf{q}})] \right\}, \quad (\text{S.27})$$

and $\Pi_q^{0z} = -\Pi_q^{z0}$. Here, $n_F(x) = [\exp(x/T) + 1]^{-1}$ is the Fermi function and we have defined $\tilde{\Delta} = \Delta - \mu$, $\epsilon_{\mathbf{q}} = t_{pp}|h_{\mathbf{q}}|$ and $g_{\pm, \mathbf{q}, \mathbf{k}} = \frac{1}{2} t_{pp}^2 (h_{\mathbf{q}}^* h_{\mathbf{q}+\mathbf{k}} \pm \text{c.c.})$. We note that the response functions $\Pi^{\alpha\beta}$ are only C_2 symmetric, but their sum as it appears in the action is always fully C_4 symmetric, which we have verified explicitly. Importantly, in the long wavelength limit, one finds that both $\lim_{|\mathbf{k}| \rightarrow 0} \Pi^{00} > 0$ and $\lim_{|\mathbf{k}| \rightarrow 0} \Pi^{zz} > 0$. This determines the sign of the biquadratic exchange coupling $K > 0$ as given in Eq. (1) of the main text.

Focusing on the bare biquadratic term arising from the product of the operators $\mathcal{S}_{\mathbf{p}, \mathbf{q}}$ in Eq. (S.23), it is instructive to write it in real space as

$$S_2^{S^2} = -\frac{J'^2}{2} \sum_{i, j} \left\{ \Pi_{ji}^{00} (\mathbf{S}_i \cdot \mathbf{S}_{i+\hat{x}} + \mathbf{S}_i \cdot \mathbf{S}_{i+\hat{y}}) (\mathbf{S}_j \cdot \mathbf{S}_{j+\hat{x}} + \mathbf{S}_j \cdot \mathbf{S}_{j+\hat{y}}) \right. \\ \left. + \Pi_{ji}^{zz} (\mathbf{S}_i \cdot \mathbf{S}_{i+\hat{x}} - \mathbf{S}_i \cdot \mathbf{S}_{i+\hat{y}}) (\mathbf{S}_j \cdot \mathbf{S}_{j+\hat{x}} - \mathbf{S}_j \cdot \mathbf{S}_{j+\hat{y}}) + 4\Pi_{ji}^{z0} (\mathbf{S}_i \cdot \mathbf{S}_{i+\hat{x}}) (\mathbf{S}_j \cdot \mathbf{S}_{j+\hat{y}}) \right\} \quad (\text{S.28})$$

with $\Pi_{ji} = \int_{\mathbf{q}} e^{-i\mathbf{q} \cdot (\mathbf{R}_j - \mathbf{R}_i)} \Pi_{-\mathbf{q}}$. The bare biquadratic exchange coupling K_0 follows as

$$K_0 = \frac{J'^2}{2} \Pi_{ii}^{zz} = \frac{J'^2}{2} \int_{\mathbf{q}} \Pi_{\mathbf{q}}^{zz}. \quad (\text{S.29})$$

We note again that the action $S_2^{S^2}$ is fully C_4 invariant and the interaction terms that involve spin operators in neighboring unit cells $i - \hat{x}$ and $i - \hat{y}$ arise from the off-diagonal components Π_{ij}^{z0} . In Fig. S.1 we show the response functions $\Pi^{\alpha\beta}$ both in real and momentum space for a realistic choice of parameters $t_{pd} = 1$, $t_{pp} = 0.2$, $\Delta = 2.5$, $n_p = 0.05$, $U_{dd} = 9$, $U_{pp} = 3$, $V_{pp} = 2.0$, $V_{pd} = 1.0$ and temperature $T = 0.02$.

S1.C. Analysis of bare biquadratic exchange coupling constant K_0

To gain some analytic understanding, we approximate the bare biquadratic coupling constant by

$$K_0 \approx \frac{J'^2}{2} \lim_{\mathbf{q} \rightarrow 0} \Pi_{\mathbf{q}}^{zz} = J'^2 \int_{BZ} \frac{d^2 q}{v_{BZ}} \frac{n_F(\xi_-) - n_F(\xi_+)}{\epsilon_{\mathbf{q}}}. \quad (\text{S.30})$$

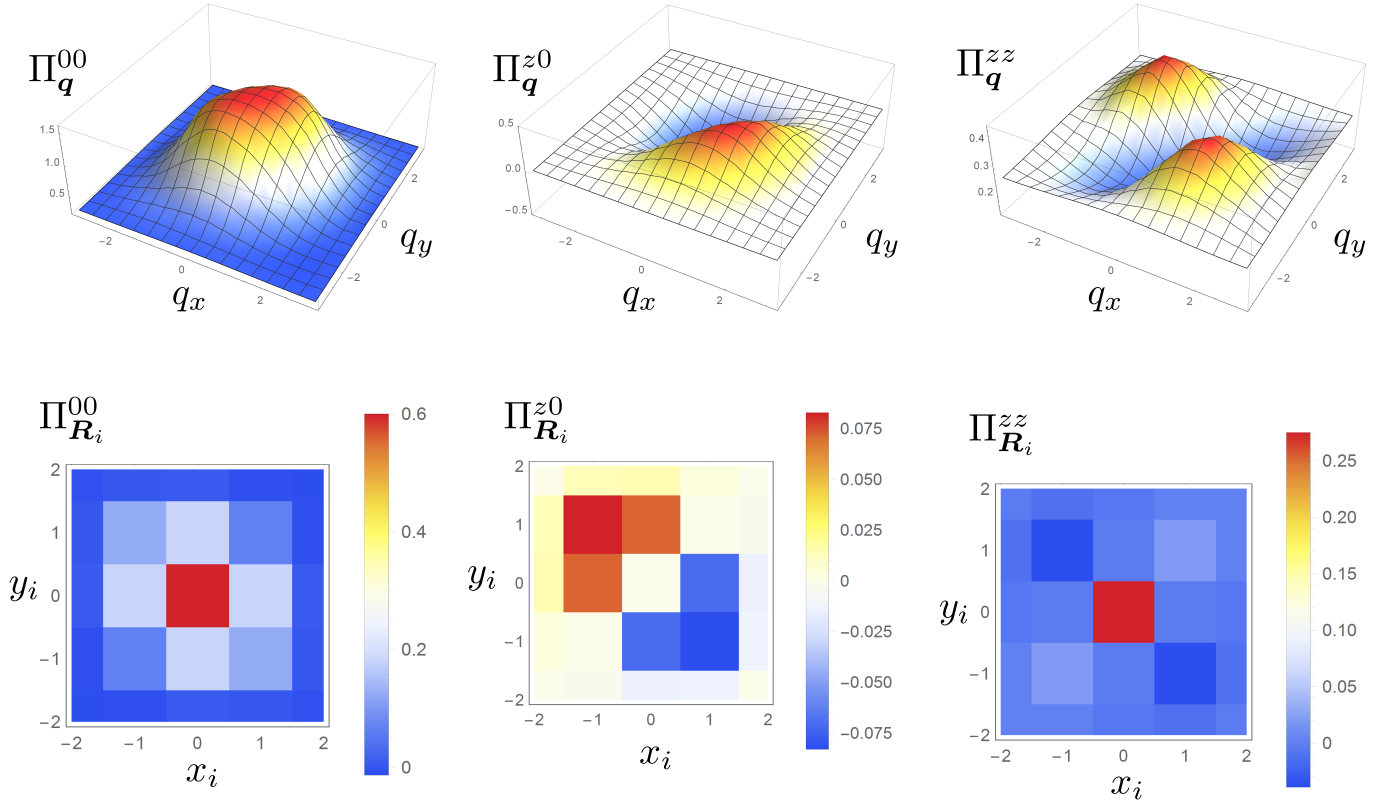


FIG. S.1. Response functions in momentum $\Pi_{\mathbf{q}}^{\alpha\beta}$ (upper row) and real-space $\Pi_{\mathbf{R}_i}^{\alpha\beta}$ (lower row). From left to right we show Π^{00} , Π^{z0} , Π^{zz} for parameters $t_{pp} = 1.0$, $T = 0.1$, $n_p = 0.1$. While $\Pi_{\mathbf{q}}^{\alpha\beta}$ are only C_2 -symmetric, the resulting expression in the action is fully C_4 -symmetric due to multiplication with the lattice functions h_m, h_η . We observe that $\Pi_{\mathbf{q}}^{zz}$ peaks at a non-zero wavevector showing that the maximal nematic response occurs at a finite \mathbf{q} .

Here, $\xi_{\pm} = \pm\epsilon_{\mathbf{q}} - \mu$ describes the two oxygen bands. Neglecting the interaction with the Néel magnetic background of the localized Cu spins, we obtain the oxygen bandstructure from the lattice function $h_{\mathbf{q}} = 1 - e^{iq_x} - e^{-iq_y} + e^{i(q_x - q_y)}$:

$$\epsilon_{\mathbf{q}} = t_{pp}|h_{\mathbf{q}}| = 4t_{pp}\left|\sin\frac{q_x}{2}\right|\left|\sin\frac{q_y}{2}\right|. \quad (\text{S.31})$$

It is useful to introduce the density of states

$$g(\epsilon) = \frac{8}{(2\pi)^2} \int_{\cos^{-1}(1-\tilde{\mu})}^{\pi} dq_x \frac{\|\dot{\alpha}(q_x)\|}{\|\nabla \xi_{\mathbf{q}=\alpha(q_x)}\|} = \frac{8}{(2\pi)^2} \frac{4i}{\tilde{\mu}} \left[K\left(\frac{4}{\tilde{\mu}^2}\right) - F\left(\frac{1}{2} \cos^{-1}(1-\tilde{\mu}), \frac{4}{\tilde{\mu}^2}\right) \right], \quad (\text{S.32})$$

where $\tilde{\mu} = \mu/(2t_{pp})$, $\alpha(q_x) = (q_x, q_y(q_x))$ with $q_y(q_x) = \cos^{-1}\left(\frac{1-\tilde{\mu}^2 - \cos q_x}{1 - \cos q_x}\right)$. The function $F(x)$ [$K(x)$] is the [complete] elliptic integral of the first kind. We note that the density of states logarithmically diverges as $\epsilon \rightarrow 0$ due to a van-Hove singularity. We can now analyze the low and high-temperature behavior of the nematic response

$$\Pi_{\mathbf{k} \rightarrow 0, \omega=0}^{zz} = \frac{1}{t_{pp}} \int_0^2 d\epsilon \frac{g(\epsilon)}{\epsilon} \frac{\sinh \frac{\epsilon}{T}}{\cosh \frac{\epsilon}{T} + \cosh \frac{\mu}{T}} = \begin{cases} \frac{g(T)(2-|\mu|)}{t_{pp}} + \frac{e^{-|\mu|/T} |\log T|}{t_{pp}}, & \text{at low } T \ll 2t_{pp} \\ \frac{1}{2Tt_{pp}}, & \text{at high } T \gg 2t_{pp}, \end{cases} \quad (\text{S.33})$$

where $2 - |\mu| \propto n_p$. At low temperatures, the response is dominated by the constant term proportional to n_p . As shown in Fig. 3 of the main text, the biquadratic exchange thus behaves in the experimentally relevant regime at low $T \ll 2t_{pp}$ as

$$\frac{K_0}{J} \propto \frac{J'^2 n_p}{J t_{pp}}. \quad (\text{S.34})$$

S1.D. Renormalization of biquadratic exchange coupling K by quadrupolar oxygen density fluctuations

We now show that quadrupolar oxygen density fluctuations further enhance the biquadratic spin exchange from its bare value K_0 to a renormalized value $K > K_0$. These oxygen density fluctuations become stronger for increasing oxygen-oxygen repulsion V_{pp} . They are described by the bosonic Hubbard-Stratonovich fields $\Phi_q = (\psi_q, \phi_q)$ defined above Eq. (S.12). In the parameter regime we consider these fluctuations are non-critical and thus remain massive. Nematic order does not develop spontaneously, but occurs only in the presence of a conjugate symmetry-breaking field such as strain or as provided by the CuO chains in YBCO. After integration over the fermionic fields $p_{qu\sigma}^\dagger$ and $p_{qu\sigma}$ the action reads (see Eq. (S.22))

$$S = \int_q \sum_{\alpha, \beta} (\Phi_q^\dagger)_\alpha (U_q)_{\alpha\beta} (\Phi_q)_\beta - \frac{1}{2} \int_q \Pi_q^{\alpha\beta} \left[(\Phi_q^*)_\alpha - \int_k \mathcal{S}_{k,-q} h_\alpha(\mathbf{k}, \mathbf{q}) \right] \left[(\Phi_q)_\beta - \int_k \mathcal{S}_{k,q} h_\beta(\mathbf{k}, -\mathbf{q}) \right], \quad (\text{S.35})$$

where $\alpha, \beta \in \{0, z\}$ and we identify $h_0(\mathbf{k}, \mathbf{q}) \equiv h_m(\mathbf{k}, \mathbf{q})$ and $h_z(\mathbf{k}, \mathbf{q}) \equiv h_\eta(\mathbf{k}, \mathbf{q})$. Performing the Gaussian integration over Φ_q^\dagger yields

$$S = S_2^{S^2} - \frac{1}{4} \sum_{\alpha, \beta, \gamma, \gamma'} \int_{q, k_1, k_2} \mathcal{S}_{k_1, q} \mathcal{S}_{k_2, q} h_\gamma(\mathbf{k}_1, -\mathbf{q}) h_{\gamma'}(\mathbf{k}_2, \mathbf{q}) (\tilde{U}_q^{-1})_{\alpha\beta} \Pi_q^{\gamma\alpha} \Pi_q^{\gamma'\beta}, \quad (\text{S.36})$$

where we have defined

$$(\tilde{U}_q)_{\alpha\beta} = (U_q)_{\alpha\beta} - \frac{1}{2} \Pi_q^{\alpha\beta} \quad (\text{S.37})$$

with U_q given in Eq. (S.11). We note that the action in Eq. (S.36) is fully C_4 symmetric after summation over $\alpha, \beta, \gamma, \gamma'$, which we have explicitly verified. We can readily extract the renormalized response functions $\tilde{\Pi}_q^{\alpha\beta}$ as

$$\tilde{\Pi}_q^{\gamma\gamma'} = \Pi_q^{\gamma\gamma'} + \frac{1}{2} \sum_{\alpha, \beta} (\tilde{U}_q^{-1})_{\alpha\beta} \Pi_q^{\gamma\alpha} \Pi_q^{\gamma'\beta}. \quad (\text{S.38})$$

The renormalized biquadratic exchange interaction is therefore determined by the zz component $\tilde{\Pi}_q^{zz} = \Pi_q^{zz} + \frac{1}{2} \sum_{\alpha, \beta} (\tilde{U}_q^{-1})_{\alpha\beta} \Pi_q^{z\alpha} \Pi_q^{z\beta}$. To gain more insight, we approximate the local response $\tilde{\Pi}_{ii}^{zz}$, which determines the biquadratic coupling $K = \frac{J'^2}{2} \tilde{\Pi}_{ii}^{zz}$ (see Eq. (S.29)), by the $\mathbf{q} = 0$ component $\tilde{\Pi}_{\mathbf{q}=0}^{zz}$. Using that $(\tilde{U}_{\mathbf{q}=0}^{-1})_{11} = \frac{1}{U_{11} - \frac{1}{2} \Pi_{\mathbf{q}=0}^{zz}}$ with $U_{11}(\mathbf{q} = 0) = \frac{1}{2} \frac{1}{V_{pp} - \frac{U_{pp}}{8}}$, the biquadratic exchange K , renormalized by quadrupolar oxygen density fluctuations, is given by

$$K = \frac{K_0}{1 - (V_{pp} - \frac{U_{pp}}{8}) \Pi_{ii}^{zz}}. \quad (\text{S.39})$$

We show K/J as a function of hole doping n_p in Fig. 2(a) of the main text for realistic parameters of the cuprates. The main insight from this result is that while on-site oxygen interactions U_{pp} tend to reduce the biquadratic exchange, repulsive oxygen-oxygen interactions V_{pp} enhance the biquadratic spin coupling $K > K_0$. For realistic parameters of the cuprates it holds that $V_{pp} \gg U_{pp}/8$ and the enhancement due to V_{pp} is the dominant effect.

S2. Nematic susceptibility within a soft-spin description of the half-filled $t - J - K$ -model

In order to obtain an analytic understanding of the nematic response in the presence of a biquadratic exchange term $\propto K$ close to a Néel ordered state, we investigate a soft-spin version of the two-dimensional t - J - K -model at half-filling. We have also analyzed the nematic susceptibility in spatial dimensions $2 < d \leq 3$ and found that the results for the nematic response from $d = 2$ remain qualitatively unchanged. After decoupling the biquadratic term at the expense of introducing the Hubbard-Stratonovich field φ_r , the action reads

$$S = \gamma \int_q \left[r_0 + q^2 + (\varphi_r + h_\varphi)(q_x^2 - q_y^2) + \gamma |\omega_n|^{2/z} \right] M_q^\alpha M_{-q}^\alpha + \frac{\gamma^3 \tilde{u}}{2N} \int_{q_1, q_2, q_3} M_{q_1}^\alpha M_{q_2}^\alpha M_{q_3}^\beta M_{-q_1 - q_2 - q_3}^\beta + \int_r \frac{N \varphi_r^2}{2g}. \quad (\text{S.40})$$

Here, $\mathbf{M}_q = (M_q^1, M_q^2, \dots, M_q^N)$ with $q = (i\omega_n, \mathbf{q})$ combining Matsubara frequency $i\omega_n = 2\pi i n T$ and momentum $\mathbf{q} = (q_x, q_y)$ denotes the (dimensionless) N -component staggered Néel magnetization. The integrations run over $\int_q = T \sum_{\omega_n} \int_{\Lambda} \frac{d^2 q}{(2\pi)^2}$ with dimensionless momentum and frequency cutoffs Λ and $\gamma\Lambda_\omega$ and $\int_r = \int_0^\beta d\tau \int d^2 r$. The coupling constant $g \propto K/J$ is proportional to the ratio of biquadratic exchange K to nearest-neighbor Heisenberg exchange J in the spin model. The (bare) mass parameter r_0 controls the distance to the quantum critical point between Néel ordered and a paramagnetic $T = 0$ phases, and $\tilde{u} = u/\gamma$ is a dimensionless interaction constant. We have rescaled the interaction term u/N to obtain a well-defined large- N limit. In the following we set the dynamic critical exponent to $z = 2$, which describes damping due to particle-hole excitations in the presence of doped holes. We have added a source field h_φ (denoted $h_r \equiv h_\varphi$ in the main text) that couples to homogeneous nematic order $\int_x h_\varphi \mathbf{M}_r (\mathbf{M}_{r+\hat{x}} + \mathbf{M}_{r-\hat{x}} - \mathbf{M}_{r+\hat{y}} - \mathbf{M}_{r-\hat{y}})$ with $\hat{x} = a_0(1, 0)$ and $\hat{y} = a_0(0, 1)$ with Cu-Cu distance a_0 .

S2.A. Nematic susceptibility $\chi_{nem,0}(r, T)$

The nematic susceptibility $\chi_{nem}(T) = \int_0^{1/T} d\tau \sum_i \langle \mathcal{T}_\tau \varphi_i(\tau) \varphi_0(0) \rangle$ in Eq. (5) of the main text is obtained from the partition function $Z = \int \mathcal{D}(\mathbf{M}_q, \varphi_r) e^{-S}$ as

$$\chi_{nem} = \frac{1}{\beta L^2} \frac{\partial^2 \ln Z}{\partial h_\varphi^2} \Big|_{h_\varphi=0} = \frac{\chi_{nem,0}}{1 - \frac{g}{N} \chi_{nem,0}} \quad (\text{S.41})$$

with inverse temperature $\beta = 1/T$ and bare nematic susceptibility

$$\chi_{nem,0} = \frac{N}{g} - \frac{1}{\beta L^2 \langle \bar{\varphi}_r^2 \rangle}. \quad (\text{S.42})$$

To obtain this expression, we have shifted the field $\bar{\varphi}_r = \varphi_r + h_\varphi$ in Eq. (S.40) before taking the derivatives with respect to h_φ and assumed the absence of an external field $h_\varphi = 0$ so that $\langle \bar{\varphi}_r \rangle^2 = 0$. We focus on static and homogeneous Hubbard-Stratonovich fields φ_r and $\bar{\varphi}_r$, *i.e.*, both fields are independent of r . To analytically calculate the expectation value $\langle \bar{\varphi}_r^2 \rangle$, we decouple the quartic term $\propto u$ in Eq. (S.40) by defining the (dimensionless) density $\rho_\psi = \frac{1}{N} \mathbf{M}_x \cdot \mathbf{M}_x$ and introducing a factor of unity as $1 = \int \mathcal{D}(\rho_\psi, \psi) e^{-\frac{1}{\gamma} \int_r (\mathbf{M}_x^2 - N \rho_\psi) \psi}$ [4], to arrive at

$$S = \gamma \int_q [r_0 + \psi + \mathbf{q}^2 + \bar{\varphi}_r(q_x^2 - q_y^2) + \gamma|\omega_n|] \mathbf{M}_q \cdot \mathbf{M}_{-q} + \frac{N}{\gamma} \int_r \frac{(\bar{\varphi}_r - h_\varphi)^2}{2\tilde{g}} + \frac{N}{\gamma} \int_r \left(\frac{\tilde{u}}{2} \rho_\psi^2 - \psi \rho_\psi \right). \quad (\text{S.43})$$

Here, the dimensionless field ψ describes the renormalization of the mass from $r_0 \rightarrow r \equiv r_0 + \psi$. Separating longitudinal and transverse components $\mathbf{M}_r = (\sqrt{N}M, \boldsymbol{\pi}_r)$, where we restrict to homogeneous magnetic order M , and integrating over the $(N-1)$ transverse components, we arrive at the action density s :

$$s \equiv \frac{S}{\beta L^2 \gamma^{-1}} = N(r_0 + \psi)M^2 + \frac{N-1}{2} \gamma \int_q \ln(r_0 + \psi + \mathbf{q}^2 + \bar{\varphi}_r(q_x^2 - q_y^2) + \gamma|\omega_n|) + \frac{N(\bar{\varphi}_r - h_\varphi)^2}{2\tilde{g}} + N \left(\frac{\tilde{u}}{2} \rho_\psi^2 - \psi \rho_\psi \right). \quad (\text{S.44})$$

Next, we expand the logarithm in small $\bar{\varphi}$ to find

$$\frac{s}{N} = \frac{\gamma}{2} \int_q \log r_q + \frac{\bar{\varphi}_r^2}{2} \left(\frac{1}{\tilde{g}} - \gamma \int_q \frac{q^4 \cos^2(2\theta)}{2r_q^2} \right) + \frac{\tilde{u}}{2} \rho_\psi^2 - \psi \rho_\psi + \mathcal{O}(\bar{\varphi}^3), \quad (\text{S.45})$$

where $\mathbf{q} = |\mathbf{q}|(\cos \theta, \sin \theta)$ and $r_q = r + q^2 + \gamma|\omega_n|$ with $r = r_0 + \psi$. The generating functional of $\bar{\varphi}_r$ then reads

$$W[h_\varphi] = \frac{1}{Z} \int \mathcal{D}(\bar{\varphi}_r) e^{-S - \bar{\varphi}_r h_\varphi} = \exp \left[\frac{h_\varphi^2}{2N} \frac{\gamma}{\beta L^2} \left(\frac{1}{\tilde{g}} - \gamma \int_q \frac{q^4 \cos^2(2\theta)}{2r_q^2} \right)^{-1} \right] \quad (\text{S.46})$$

and the bare nematic susceptibility $\chi_{nem,0}$ in Eq. (S.42) follows to

$$\chi_{nem,0} = \frac{N}{2} T \sum_{\omega_n} \int_0^\Lambda \frac{d^2 q}{(2\pi)^2} \frac{q^4 \cos^2(2\theta)}{(r + q^2 + \gamma|\omega_n|)^2} = \frac{N}{(2\pi)^2 \gamma} \int_0^{\gamma\Lambda_\omega} d\omega \int_0^\Lambda dq \frac{\omega(r + q^2) q^5}{[(r + q^2)^2 + \omega^2]^2} \coth\left(\frac{\omega}{2\gamma T}\right). \quad (\text{S.47})$$

In the final step we have gone from summation over Matsubara frequencies to integration along the real frequency axis, and performed the angular integration over θ . Note that while ω_n has units of energy, the integration variable

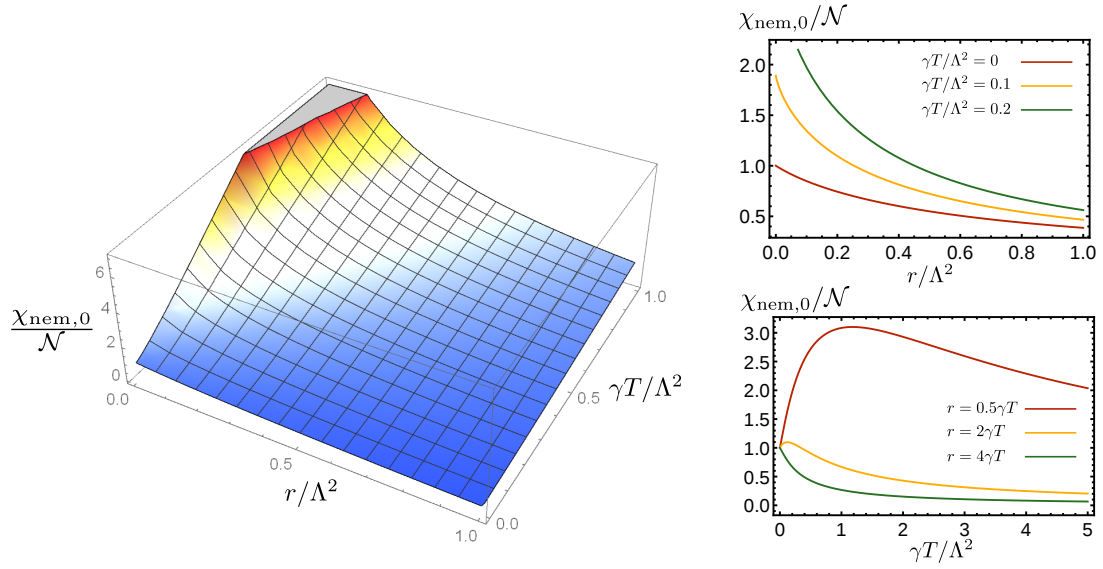


FIG. S.2. (Left) Nematic susceptibility $\chi_{\text{nem},0}/\mathcal{N}$ with cutoff dependent normalization factor $\mathcal{N} = N\Lambda^4/(64\pi^2\gamma)$ as a function of $\tilde{r} = r/\Lambda^2$ and $\tilde{T} = \gamma T/\Lambda^2$. We observe that for fixed temperature T , the susceptibility increases as $r \propto \xi^{-2}$ decreases (see panel on the upper right). This shows that Néel fluctuations enhance the nematic susceptibility. As a function of temperature, we observe that $\chi_{\text{nem},0}/\mathcal{N}$ starts out from a non-zero value at $T = 0$ that is equal to $\chi_{\text{nem},0}(r = 0, T = 0)/\mathcal{N} = 1$ at the quantum critical point and smaller for $r > 0$. The finite-temperature behavior of $\chi_{\text{nem},0}[r(T), T]/\mathcal{N}$ depends on microscopic details as expected for a non-universal quantity. The panel on the lower right shows the finite- T behavior above the quantum critical point for different values of the slope $r(T) = a\gamma T$, $a = \{0.5, 2, 4\}$. For $a < \pi$ ($a > \pi$) the susceptibility first increases (decreases) linearly as a function of T , at larger T it decays to zero. It reaches a maximum when $\tilde{r} \approx 1$, which marks the transition into the lattice high- T regime.

ω is dimensionless by expressing energies in units of γ^{-1} . While we must keep both momentum and frequency cutoff Λ and $\gamma\Lambda_\omega$ finite when we solve for $r(r_0, T)$ in the following section (using the large- N approximation), we may take the limit $\gamma\Lambda_\omega \rightarrow \infty$ in Eq. (S.47). This allows us to exactly perform the momentum and frequency integrations and completely absorb the cutoff Λ by expressing $\chi_{\text{nem},0}$ in terms of the (dimensionless) variables $\tilde{r} = r/\Lambda^2$ and $\tilde{T} = \gamma T/\Lambda^2$ as

$$\chi_{\text{nem},0} = \frac{N\Lambda^4}{64\pi^2\gamma} \left[4\pi\tilde{T} \left[\frac{2\tilde{r}+1}{\tilde{r}+1} + 2\tilde{r} \log \frac{\tilde{r}}{\tilde{r}+1} \right] + 2\psi \left(1 + \frac{\tilde{r}+1}{2\pi\tilde{T}} \right) - 8\pi\tilde{T} \left\{ \log \Gamma \left(\frac{\tilde{r}+1+2\pi\tilde{T}}{2\pi\tilde{T}} \right) + 2\pi\tilde{T} \left[\psi^{(-2)} \left(1 + \frac{\tilde{r}}{2\pi\tilde{T}} \right) - \psi^{(-2)} \left(1 + \frac{r+1}{2\pi\tilde{T}} \right) \right] \right\} \right]. \quad (\text{S.48})$$

In Fig. S.2, we show $\chi_{\text{nem},0}/\mathcal{N}$, where $\mathcal{N} = N\Lambda^4/(64\pi^2\gamma)$ as a function of $\tilde{r} = r/\Lambda^2$ and $\tilde{T} = T/\Lambda^2$. Note that $\mathcal{N} \equiv \chi_{\text{nem},0}(r = 0, T = 0)$ is the value of the susceptibility at the quantum critical point. Along a path of constant temperature, the nematic susceptibility increases as r decreases, which is also shown in the upper right panel of Fig. S.2. Decreasing $r \propto \xi^{-2}$ implies an increasing magnetic Néel correlation length as one approaches the $T = 0$ quantum critical point or the renormalized classical regime with exponentially large magnetic correlation length at $T > 0$. The nematic susceptibility thus increases as a result of larger magnetic Néel fluctuations. Our analysis also reveals that while for classical spins $\chi_{\text{nem},0}$ vanishes as $T \rightarrow 0$, quantum fluctuations render the zero temperature limit of $\chi_{\text{nem},0}$ finite.

To plot $\chi_{\text{nem},0}$ along a path of constant r_0 , which controls the distance to the quantum critical point beyond which Néel order disappears, one needs to solve for the renormalized mass parameter $r(T, r_0)$. At finite temperatures above the quantum critical point, one finds $r(T, r_{0,c}) = a\gamma T \propto T$ with a non-universal proportionality constant a that depends on microscopic details of the system. As shown in the lower right panel of Fig. S.2, the shape of $\chi_{\text{nem},0}$ crucially depends on the value of the slope parameter a , which controls the relative importance of quantum and thermal fluctuations. For small values of $a < \pi$, $\chi_{\text{nem},0}$ develops a pronounced finite-temperature peak, whose amplitude increases with decreasing a . This behavior of $\chi_{\text{nem},0}$ closely resembles the behavior found within the classical Monte-Carlo simulations (see Fig. 2 of the main text), and show that thermal fluctuations are dominant for $a < \pi$. In contrast, for larger values $a > \pi$, $\chi_{\text{nem},0}$ peaks at $T = 0$ and is a monotonically decreasing function for

finite T , showing the dominance of quantum fluctuations in this case.

S2.B. Large- N analysis of the nematic susceptibility

In order to determine the effective mass parameter $r(T, \delta r_0)$ as a function of temperature T and distance to the quantum critical point $\delta r_0 = r_0 - r_{0,c}$, we consider the limit of large- N , where the partition function is governed by the saddle point of the action in Eq. (S.40). Finding the saddle-point of the action in Eq. (S.44) in the absence of nematic order, leads to the well-known large- N self-consistency equations [4, 5]: $rM = 0$ with $r = r_0 + \psi$; $\rho_\psi = \gamma\psi/u$ and

$$r = r_0 + uM^2 + \frac{u}{2} \int_q \frac{1}{r + q^2 + \gamma|\omega_n|} \quad (\text{S.49})$$

The equation requires a finite frequency cutoff Λ_ω . For the results of $\chi_{\text{nem},0}$ in Fig. 2 of the main text, we have therefore numerically solved these equations for finite momentum Λ and (dimensionless) frequency cutoffs $\gamma\Lambda_\omega$, which yields $r(r_0, T)$ shown in Fig. S.3. The qualitative behavior of $\chi_{\text{nem},0}$ as discussed in the previous section does not depend on the exact value of $\gamma\Lambda_\omega$ and Λ as long as both cutoffs are much larger than $r, \gamma T \ll \Lambda, \gamma\Lambda$.

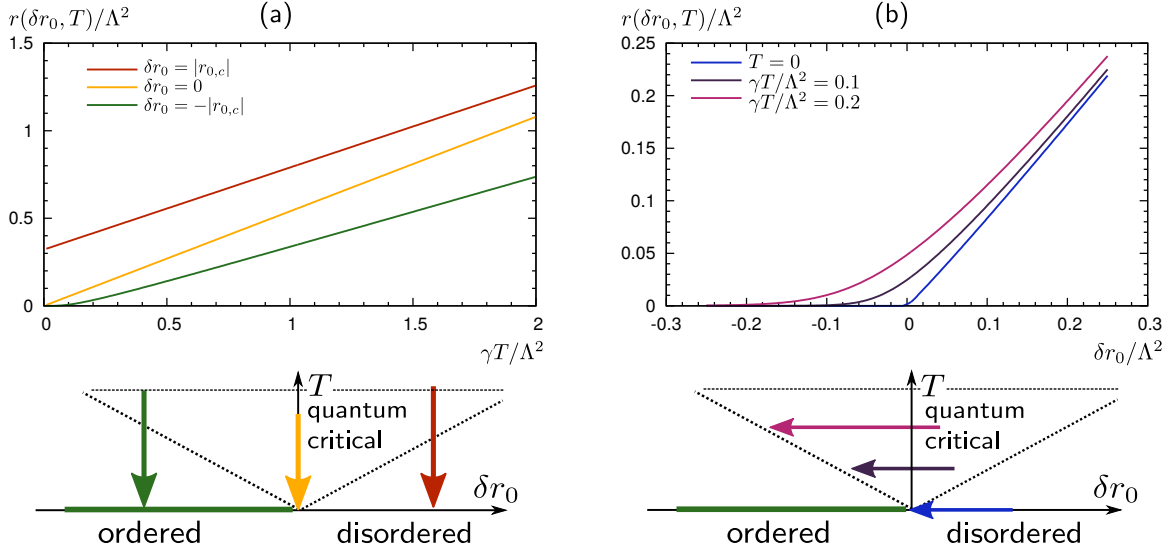


FIG. S.3. Large- N solutions for the “mass” parameter $r(r_0, T) \propto \xi^{-2}$, where ξ is the magnetic correlation length for Néel order. This parameter controls the distance to criticality. The resulting nematic susceptibilities are shown in Fig. 3 of the main text. Panels (a) and (b) correspond to same panels in Fig. 3 of the main text. The left panel (a) shows r as a function of temperature at fixed distance to criticality δr_0 , as depicted in the schematic diagram with vertical paths corresponding to different values of δr_0 . For $\delta r_0 > 0$ (red), r approaches a finite value as $T \rightarrow 0$ corresponding to a finite magnetic correlation length in the quantum disordered phase. In contrast, for $\delta r_0 \leq 0$ (yellow, green), $r \rightarrow 0$ as $T \rightarrow 0$. Approaching the quantum critical point (yellow), one finds $r = a\gamma T$ with non-universal slope a that depends among others on the size of the interactions u/γ . Larger u/γ yields a larger a . Approaching the magnetically ordered phase (green), we observe a change in functional behavior of $r(T)$ as we cross from the quantum critical to the renormalized classical regime. In the quantum critical regime at higher T , one finds $r(T) \propto T$. In contrast, in the renormalized classical regime at lower T , it holds $r(T) \propto T \exp(-\Delta(\delta r_0)/T)$, where Δ depends on the spin stiffness in the ordered phase (rigidity towards magnetic fluctuations) [5]. The right panel (b) corresponds to changing δr_0 at fixed temperature T . In an experiment, this corresponds, for example, to tuning the chemical composition or pressure. Importantly, we observe that $r \propto \xi^{-2}$ is a monotonously decreasing function for decreasing δr_0 , *i.e.*, approaching the quantum critical point or the renormalized classical region. While in two dimensions the Hohenberg-Mermin-Wagner theorem ensures a finite correlation length $r > 0$ at any finite temperature T , one finds that $r(T)$ becomes exponentially small, because ξ becomes exponentially large, in the renormalized classical regime to the left of the dashed line. From Fig. 2 of the main text, we conclude that the nematic susceptibility χ_{nem} increases if r decreases or ξ increases, which shows that larger Néel fluctuations enhance the nematic response.

S3. Spin-wave treatment of $t - J - K$ model at half-filling

At half-filling the Hamiltonian in Eq. (1) of the main text describes localized Cu spins interacting via nearest-neighbor Heisenberg exchange interaction J and a biquadratic exchange interaction K . Additional weaker next-nearest neighboring and ring-exchange terms may be added to obtain agreement with the experimental spin-wave spectra [6]. Since these terms do not change our conclusions, we do not explicitly consider them below. Note that we include a realistic ferromagnetic exchange coupling $J_2 = -0.1J$ in our Monte-Carlo simulations (see Fig. 2 of the main text).

We now show that the biquadratic spin exchange term $\propto K$ does not modify the spin-wave spectrum. Adding such a term in the Hamiltonian is thus fully consistent with previous experimental results of the spin-wave spectrum. We derive our results starting from the J - K model spin Hamiltonian in Eq. (1) of the main text

$$H = \frac{J}{2} \sum_{i=1}^{N_L} \sum_{\delta_\nu=\delta_1}^{\delta_4} \mathbf{S}_i \mathbf{S}_{i+\delta_\nu} - \frac{K}{4S^2} \sum_{i=1}^{N_L} \left[\mathbf{S}_i \left(\mathbf{S}_{i+\hat{x}} + \mathbf{S}_{i-\hat{x}} - \mathbf{S}_{i+\hat{y}} - \mathbf{S}_{i-\hat{y}} \right) \right]^2. \quad (\text{S.50})$$

Here, $\{\delta_\nu\} = \{\pm\hat{x}, \pm\hat{y}\}$ connect nearest-neighbors Cu sites. Let us calculate the spin-wave spectrum around the Néel state. As this corresponds to a large- S limit, we have rescaled the biquadratic term. We follow the standard procedure of Holstein-Primakoff spin-wave calculations [7] and begin with defining local triads $\mathbf{n}_{1,\mathbf{R}_i} = (\cos(\mathbf{Q} \cdot \mathbf{R}_i), 0, -\sin(\mathbf{Q} \cdot \mathbf{R}_i))$, $\mathbf{n}_2 = (0, 1, 0)$ and $\mathbf{n}_{3,\mathbf{R}_i} = (\sin(\mathbf{Q} \cdot \mathbf{R}_i), 0, \cos(\mathbf{Q} \cdot \mathbf{R}_i))$ with Néel ordering wavevector $\mathbf{Q} = (\pi, \pi)$. Expressing the spins in terms of this local coordinate system $\mathbf{S}_i = \sum_\alpha \tilde{S}_i^\alpha \mathbf{n}_{\alpha,\mathbf{R}_i}$, the Hamiltonian takes the form (suppressing the tilde)

$$H = \frac{J}{2} \sum_{i,\delta_\nu,\alpha,\beta} S_i^\alpha S_{i+\delta_\nu}^\beta n_{\beta,\delta_\nu}^\alpha + \frac{K}{4S^2} \sum_i \sum_{\alpha,\beta} \left[n_{\beta,\delta_\nu}^\alpha S_i^\alpha \left(S_{i+\hat{x}}^\beta + S_{i-\hat{x}}^\beta - S_{i+\hat{y}}^\beta - S_{i-\hat{y}}^\beta \right) \right]^2 \quad (\text{S.51})$$

with $n_{\beta,\delta_\nu}^\alpha = \delta_{\alpha\beta}(-\delta_{x\alpha} + \delta_{y\alpha} - \delta_{z\alpha})$. A transformation to momentum space via $\mathbf{S}_i = \frac{1}{\sqrt{N_L}} \sum_{\mathbf{p} \in BZ} e^{i\mathbf{p} \cdot \mathbf{R}_i} \mathbf{S}_{\mathbf{p}}$ yields

$$H = 2J \sum_{\mathbf{p}} \sum_{\alpha} f_{\mathbf{p}} S_{\mathbf{p}}^\alpha S_{-\mathbf{p}}^\alpha n_{\alpha,\delta_\nu}^\alpha + \frac{K}{N_L S^2} \sum_{\mathbf{p},\mathbf{q},\mathbf{k}} \sum_{\alpha,\beta} S_{\mathbf{p}+\mathbf{k}}^\alpha S_{-\mathbf{p}}^\alpha S_{\mathbf{q}-\mathbf{k}}^\beta S_{-\mathbf{q}}^\beta n_{\alpha,\delta_\nu}^\alpha n_{\beta,\delta_\nu}^\beta (\cos p_x - \cos p_y)(\cos q_x - \cos q_y), \quad (\text{S.52})$$

where we have defined the lattice function $f_{\mathbf{p}} = \frac{1}{4} \sum_{\delta_\nu} e^{-i\mathbf{p} \cdot \delta_\nu} = \frac{1}{2}(\cos p_x + \cos p_y)$. To obtain the spin-wave spectrum, we now express spin operators in terms of Holstein-Primakoff bosons $S_{\mathbf{q}}^x = \sqrt{\frac{S}{2}}(b_{-\mathbf{q}}^\dagger + b_{\mathbf{q}})$, $S_{\mathbf{q}}^y = i\sqrt{\frac{S}{2}}(b_{-\mathbf{q}}^\dagger - b_{\mathbf{q}})$ and $S_{\mathbf{q}}^z = \sqrt{N_L} S \delta_{\mathbf{q},0} - \frac{1}{\sqrt{N_L}} \sum_{\mathbf{k}} b_{\mathbf{k}-\mathbf{q}}^\dagger b_{\mathbf{k}}$. The classical ground state energy follows as the $\mathcal{O}(S^2)$ -term to $H^{(S^2)}/(N_L S^2) = -2J$. Note that the energy of the biquadratic term vanishes in the Néel state.

The next lowest order in S is quadratic in the bosons and yields upon diagonalization the spin-wave spectrum. Keeping the quadratic terms, yields

$$H_J^{(S)} = 2JS \sum_{\mathbf{q}} \left(2b_{\mathbf{q}}^\dagger b_{\mathbf{q}} - f_{\mathbf{q}}(b_{-\mathbf{q}}^\dagger b_{\mathbf{q}}^\dagger + b_{\mathbf{q}} b_{-\mathbf{q}}) \right) \quad (\text{S.53})$$

$$H_K^{(S)} = 0, \quad (\text{S.54})$$

Most importantly, according to Eq. (S.54), the biquadratic term does not contribute to the spin-wave spectrum at order $\mathcal{O}(S)$. Intuitively, the vanishing of the biquadratic contribution to the spin-wave spectrum follows from the observation that inserting the classical spin state into one of the factors $\mathbf{S}_i(\mathbf{S}_{i+\hat{x}} + \mathbf{S}_{i-\hat{x}} - \mathbf{S}_{i+\hat{y}} - \mathbf{S}_{i-\hat{y}})$ gives zero, because the term in the brackets vanishes in the Néel state. More explicit, this result can be seen already from Eq. (S.52): to obtain a term of $\mathcal{O}(S)$ the term in the bracket has to be of order S^3 in order to combine with the prefactor K/S^2 to a term of $\mathcal{O}(S)$. There are two possibilities, which both vanish: (i) $zzzz$ terms, *i.e.*, selecting 3 Kronecker symbols and selecting one term of the form $\sum_{\mathbf{k}} b_{\mathbf{k}-\mathbf{q}}^\dagger b_{\mathbf{k}}$ (from $S_{\mathbf{q}}^z$). The Kronecker symbols enforce $\mathbf{p} = \mathbf{q} = \mathbf{k} = 0$ and therefore $\cos p_x - \cos p_y = 0$ and $\cos q_x - \cos q_y = 0$. The other possibility are (ii) terms of the form $(zzxx + zzyy + xxzz + yyzz)$, *i.e.*, selecting two Kronecker symbols and two S^x, S^y terms. The Kronecker symbols give either $\mathbf{p} = \mathbf{k} = 0$ or $\mathbf{q} = \mathbf{k} = 0$ and thus one of the cos-terms vanishes: $\cos p_x - \cos p_y = 0$ or $\cos q_x - \cos q_y = 0$.

We finally want to note an interesting observation. If one uses the well-known relations for spin-1/2 operators $(\mathbf{S}_i \cdot \mathbf{S}_j)^2 = \frac{3}{16} - \frac{1}{2} \mathbf{S}_i \cdot \mathbf{S}_j$ and $(\mathbf{S}_i \cdot \mathbf{S}_j)(\mathbf{S}_i \cdot \mathbf{S}_k) = \frac{1}{4} \mathbf{S}_j \cdot \mathbf{S}_k + \frac{i}{2} \mathbf{S}_i \cdot (\mathbf{S}_j \times \mathbf{S}_k)$, one may rewrite the biquadratic term as a sum of three spin exchange terms such that the spin Hamiltonian in Eq. (S.50) takes the form

$$H = \frac{1}{2} \left(J + \frac{K}{4S^2} \right) \sum_i \sum_{\delta} \mathbf{S}_i \cdot \mathbf{S}_{i+\delta} + \frac{K}{8S^2} \sum_i \sum_{\delta'} \mathbf{S}_i \cdot \mathbf{S}_{i+\delta'} - \frac{K}{16S^2} \sum_i \sum_{\delta''} \mathbf{S}_i \cdot \mathbf{S}_{i+\delta''}. \quad (\text{S.55})$$

Interestingly, there now appears a non-zero contribution of the K -dependent exchange terms to the spin-wave spectrum. Note that this explicitly shows that using the above spin transformation rules valid for spin-1/2 does not commute with taking the large- S limit to derive the spin-wave spectrum.

S4. Details on the Monte-Carlo simulations

The Monte Carlo simulations were carried out at 100 equally spaced temperature points in the interval $0.001 < T/J < 2.971$. We applied a combination of single-move Metropolis Monte Carlo steps and non-local parallel-tempering-exchange steps between neighboring temperature configurations. The simulations shown in Fig. 2 of the main text were carried out for systems of 40×40 spins and biquadratic exchange couplings $K/J = \{0.0, 0, 35, 0.45\}$. We consider a ferromagnetic next-nearest-neighbor exchange coupling $J_2 = -0.1J$ as well. Note that the ground state phase transition in the classical model between Néel and collinear order occurs at $J/2 = J_2 + K$. Following thermalization, the averages were computed for each temperature with at least 4.5×10^6 Monte Carlo sweeps (MCS). The error bars were estimated by using the well-known Jackknife procedure.

-
- [1] V. J. Emery, [Phys. Rev. Lett. **58**, 2794 \(1987\)](#).
 - [2] E. Kolley, W. Kolley, and R. Tiertz, *J. Phys. C* **4**, 3517 (1992).
 - [3] J. Zaanen and A. M. Oleś, [Phys. Rev. B **37**, 9423 \(1988\)](#).
 - [4] J. Zinn-Justin, *Quantum Field Theory and Critical Phenomena* (Oxford University Press, New York, NY, USA, 2002).
 - [5] S. Sachdev, *Quantum Phase Transitions* (Cambridge University Press, Cambridge, U.K., 1999).
 - [6] R. Coldea, S. M. Hayden, G. Aeppli, T. G. Perring, C. D. Frost, T. E. Mason, S.-W. Cheong, and Z. Fisk, [Phys. Rev. Lett. **86**, 5377 \(2001\)](#).
 - [7] A. Auerbach, *Interacting Electrons and Quantum Magnetism* (Springer-Verlag, New York, 1994).